



HAL
open science

Bayesian networks for assessment of disruption to school systems under combined hazards

Ahsana Parammal Vatteri, Dina d'Ayala, Pierre Gehl

► To cite this version:

Ahsana Parammal Vatteri, Dina d'Ayala, Pierre Gehl. Bayesian networks for assessment of disruption to school systems under combined hazards. *International Journal of Disaster Risk Reduction*, 2022, 74, pp.102924. 10.1016/j.ijdr.2022.102924 . hal-03669417

HAL Id: hal-03669417

<https://brgm.hal.science/hal-03669417>

Submitted on 16 May 2022

HAL is a multi-disciplinary open access archive for the deposit and dissemination of scientific research documents, whether they are published or not. The documents may come from teaching and research institutions in France or abroad, or from public or private research centers.

L'archive ouverte pluridisciplinaire **HAL**, est destinée au dépôt et à la diffusion de documents scientifiques de niveau recherche, publiés ou non, émanant des établissements d'enseignement et de recherche français ou étrangers, des laboratoires publics ou privés.



ELSEVIER

Contents lists available at [ScienceDirect](https://www.sciencedirect.com)

International Journal of Disaster Risk Reduction

journal homepage: www.elsevier.com/locate/ijdr

Bayesian networks for assessment of disruption to school systems under combined hazards

Ahsana Parammal Vatteri^a, Dina D'Ayala^{a,*}, Pierre Gehl^b

^a University College London, London, UK

^b Expert in Earthquake Engineering, BRGM, France

ARTICLE INFO

Keywords:

School safety
Bayesian networks
Combined hazards
Education disruption
Confined masonry
System modelling

ABSTRACT

Exposure of school buildings to floods and earthquakes poses significant risk to the vulnerable population of students and their education process. In regions of high exposure, these hazards may often act concurrently, whereby yearly flood events weaken masonry school buildings, rendering them more vulnerable to frequent earthquake shaking. This recurring damage, combined with other functional losses, ultimately result in disruption to education delivery. The socio-economic condition of the users-community also plays a role in the extent of such disruption. A complex problem of this nature demands consideration of a large number of dimensions, to estimate the impact to the school system infrastructure in a locality. To handle the qualitative and quantitative nature of these variables, a Bayesian network (BN) model is proposed representing multiple schools in a locality as a system. Three dimensions are considered to contribute to the system disruption, namely, schools' physical functionality loss, accessibility and use loss, and social vulnerability. The impact is quantified through the probability of the system being in various states of disruption. The BN also explores mitigating measures, such as the mobility of students between schools in the system. The general methodology is illustrated by a case-study of school buildings in Guwahati, India, whereby the majority of buildings is constructed in confined masonry with varying level of seismic performance. The physical effects of combined flood and seismic action on confined masonry buildings is assessed by nonlinear numerical modelling, and their probabilistic occurrence is expressed in terms of fragility functions corresponding to varying flood depth and peak ground acceleration.

1. Introduction

Multi-hazard risk assessment for critical infrastructure is an integral part of disaster risk reduction from natural hazards. Increasing evidence from around the world highlights the necessity of considering concurrent or sequential hazards in the assessment of disaster risk [1], as the effects of a damaging event overlap with the effects of another in space and time windows. Hence, techniques for assessing the performance of school infrastructure under multiple hazards is highly encouraged by the Sendai Framework [2] to ensure continuity of education delivery.

In the above context, this study proposes a framework for risk assessment of the school system in a district (a set of several schools of different capacity and schooling level) from sequential flood and seismic hazards, in terms of overall disruption to school education delivery to the community that it serves. The framework is based on Bayesian Networks (BN), and the methodology is illustrated by

* Corresponding author.

E-mail addresses: ahsana.vatteri.17@ucl.ac.uk (A.P. Vatteri), d.dayala@ucl.ac.uk (D. D'Ayala), p.gehl@brgm.fr (P. Gehl).

application to a case-study of confined masonry school buildings in Guwahati, India. The case-study location, Guwahati city in Assam, is situated in India's seismic zone V, the highest risk zone by Indian Standard 1893 [3], having witnessed 20 earthquakes of $M \geq 7$ in the past 150 years [4–6]. The city is also affected by annual monsoonal and fluvial floods, making it a suitable choice for a multi-hazard risk study. A desk study of Guwahati city school infrastructure [7] and field visits identified 75% of the buildings being of masonry construction, of which more than 60% being confined to various extent, making this the predominant typology. Annual floods in the city are observed to be not large enough to cause structural collapse, nonetheless, repeated floods have a degrading effect on the masonry courses below flood depth.

The following subsections introduce the four key areas of investigation, which underpin the methodology of this study, namely, 1) the issue of education disruption immediately after a major hazard event, 2) physical vulnerability of the confined masonry school buildings to flood and seismic hazards, 3) social vulnerability and 4) use of Bayesian networks to determine the causal links between the performance of the school system in delivering education and the three above domain variables.

1.1. Disruption to education from earthquakes and floods

Large earthquakes and frequent floods cause physical damage to school infrastructure and cause interruption to the education process, as frequently observed from past events. Evidence from the past 30 years (Spitak (1988) 6.8 M_s to Indonesia (2018) 7.5 M_w) reports seismic collapse and damage of school buildings, resulting in casualties and disruption to schooling for long periods [8–10]. School children are thus identified as the most vulnerable population in earthquakes [8], while it is recognised that school architecture renders school buildings prone to damage from earthquakes [11].

While disruptive earthquakes are rare events, floods are the most common natural hazard in the world [12], and their severity and frequency is increasing, amplified by climate change. Recurring floods disrupt education by causing physical damage to the school infrastructure, affecting the organisational structure, requiring the use of schools as temporary shelters and negatively affecting wellbeing of individuals and communities [13]. Persistent issues of disruption to education associated with flooding are reported worldwide, including Kenya [14], Zimbabwe [15] and Philippines [16]. During the South-Asian floods of 2017, more than 18,000 schools were damaged in the north and north-east of India, Nepal and Bangladesh [17], affecting over 1.8 million children. Closure of schools for long periods often leads to high rates of education drop-out, especially in poor communities and when schools are used as shelters [18].

The period of disruption to education is found to vary widely after disasters, for example, it often takes many weeks and even months for the schools to resume full operation after a heavy flood event in India [19–21]. Even though many countries including India, Philippines, Japan, Fiji etc., use schools for immediate evacuation and sheltering of displaced people [22] such use is controversial, and if prolonged, causes damage to buildings and service lines further delaying the education process and quality.

It is therefore evident that education continuity is just as critical an indicator of school system performance to multiple hazards, as it is the robustness and resilience of the building forming such system. Development of tools to cater for multi-hazard risk assessment that incorporate structural and functional indicators of the school infrastructure system are therefore critically needed, and Bayesian networks (BN) provide the framework to integrate quantitative and qualitative information for a complex system model [23].

1.2. Physical vulnerability of masonry school buildings against seismic and flood hazards

Acknowledging the need for vulnerability assessment in the specific context of school buildings, extensive analytical studies have been reported, especially in the context of structural vulnerability under seismic hazard. Seismic vulnerability assessment of schools generally involves a three-tier approach as follows: a first level of Rapid Visual Screening (RVS) on the building population, followed by simplified vulnerability assessment using vulnerability indices or scores, and finally a detailed analytical vulnerability analysis on chosen buildings [24,25]. While large scale studies conduct the vulnerability assessment at the first and second tiers [11,26–34], more in-depth studies extend the analysis to the third tier [35–40], by deriving complete load-deflection characteristics of the building by dynamic/time-history analysis, considering intensity measures such as peak ground acceleration [41]. In addition, post-disaster reconnaissance surveys [42–44] and empirical vulnerability assessment for school buildings based on damage data [45,46] are also reported in literature. In contrast to seismic vulnerability assessment, flood vulnerability studies on schools highlighted loss of accessibility, change of use as temporary shelters and influence of socio-economic status, as major contributors to loss of functionality of schools, in addition to the physical damage to school buildings [13,14,47–49].

When considering the impact of hazards at urban or regional scale, use is made of fragility and vulnerability functions, representing damage probabilities and associated costs, conditioned to hazard intensity. The current study focuses on confined masonry school buildings for physical vulnerability analysis. Extensive experimental and numerical work exists on seismic capacity assessment of confined masonry structures, (e.g. Refs. [50–55]). For a comprehensive review of methods for out-of-plane and in-plane assessment of confined masonry school structures, the reader is directed to Parammal Vatteri and D'Ayala (2021) [56], which details the numerical analysis-based procedure for fragility assessment of selected confined masonry typologies, which is adopted in the present study.

Conversely, capacity and vulnerability assessment of masonry walls under lateral flood loading is an under-researched area, even though floods are common and frequently recurring. The lateral capacity of masonry walls under flood loading has been assessed using the yield line approach [57,58]. Kelman and Spence (2003) [57] concluded that the critical hydrostatic water depth is about 1–1.5 m for unreinforced masonry wall without opening, which can reduce to 0.5 m when realistic flow velocity is considered. Herbert et al. (2013) [58,59] conducted experimental and analytical studies on walls loaded by hydrostatic, hydrodynamic and uniform loads, considering both frictional and flexural strength, obtaining results comparable with Kelman and Spence (2003). While few numerical studies on the effect of uniform lateral pressure on masonry walls, using finite element approach are available in literature [60–62], physically based numerical analysis of masonry walls subjected to flood lateral loading has received little attention [63]. The present

study addresses this research gap by developing suitable numerical models in Applied Elements Analysis [64].

In the case of floods, the intensity measures considered for fragility and vulnerability assessment are depth and duration of inundation, velocity of floodwater flow, etc. [65], and their associated uncertainty [66]. Empirical flood fragility methods such as RiskScape [65], define correlation functions between flood depth and damage for various building typologies, based on past events. Index-based empirical vulnerability assessment tools, such as PARNASSUS V1.0 [67] and V3.0 [68] define a set of vulnerability indicators to quantify the flood vulnerability of building typologies and determine the risk associated with specific flood return periods. Mebarki et al. (2012) [69] developed a probabilistic model for flood vulnerability of masonry building at regional scale, by considering the random nature of load and strength variables. Blanco-Vogt and Schanze (2014) [70] developed a conceptual and methodological framework including economic, ecological, institutional and social aspects, to assess physical vulnerability of buildings to floods. Given the lack of high fidelity models for fragility assessment of masonry structures exposed to flooding, such modelling is develop in this study, considering hydrostatic loads from flood inundation, while ignoring other effects associated with flow velocity, impact and buoyancy.

Investigation on masonry buildings subjected to combined flood and seismic hazards is very rare [71], even more so when considering combined effects. A few studies have examined seismic and flood effects and risk assessment in the context of disaster risk reduction, such as Dabbeek et al. (2020) [72], however, quantification and comparison of their effects on building vulnerability is not common [73]. de Ruyter et al. (2017) [74] reviewed empirical vulnerability assessment techniques used for seismic or flood hazards and suggested that greater homogenization of the two fields of work is needed, using common indicators. The necessity for developing techniques for combined flood-seismic fragility assessment of buildings is therefore evident.

1.3. Social vulnerability to flood and seismic hazards

Social vulnerability, encompassing socioeconomic and demographic factors, defines the response of communities to natural hazards, through their interaction with multiple physical infrastructure systems [75,76]. It is recognised that socially vulnerable communities are disproportionately negatively impacted by natural hazards [73]. Schools being an integral part of any community, social vulnerability of the community affects the performance of schools, especially in the face of damaging and disruptive events, and vice versa, the resilience of the school system can positively reduce the impact of hazardous events on their community. A number of factors are identified to influence the social vulnerability of a community, including economic status, education level, age, disabilities, minority status or vulnerable groups, housing conditions, access to transportation, health and education infrastructure etc. [75,77,78]. Studies have shown that low income and low levels of education are major indicators of vulnerability and to an extent correlated [77]. Several studies quantify social vulnerability through summative indices that capture the states of the influencing factors, although they might suffer from biases [79–81].

Economically poorer sections of society are more likely to suffer from a natural destructive event, owing to reduced risk perception, lack of preparedness and ability to respond and recover [82]. The nexus between social vulnerability and flood and seismic vulnerability of the physical environment has been identified by several authors [47,70,83]. Socially vulnerable communities tend to live in comparatively more hazardous areas, such as the flood plains of a region, or near major faults, because of land values, therefore their schools can be less accessible after an event, even if they are physically safe to operate [18]. In such communities, the chance of schools being used as shelters is also high, as houses are more likely to be damaged or unsafe, leading to long periods of disruption to education. Communities who depend heavily on climate sensitive means of income, such as farming and fishing, disrupted during flooding events, often engage children to assist the household income and chores, leading to higher rates of school drop-out [15]. Young girls in these circumstances are often forced to child marriage [84], in an attempt to survive.

This study defines the social vulnerability of the community associated with the school system under analysis by two factors which are school-specific, the number and the age group of the students population, and two factors, income and education level of their parents, which are community specific. While it is acknowledged that this is not an exhaustive description of the complex interplay of factors determining social vulnerability, this approach allows defining the interaction of community to school infrastructure, and to illustrate the integration of multiple qualitative and quantitative factors using Bayesian networks to estimate the impact of natural hazards on such infrastructure.

1.4. Bayesian Networks for system performance modelling

Bayesian Network (BN) allows modelling complex systems with uncertainties, in order to obtain probabilities of system performance to described hazards' occurrence. The BN approach involves designing the network of variables in a problem, establishing their causal relationships in terms of *parent* and *child*. Each variable can have multiple states of existence and a conditional probability table (CPT) that defines the conditional probability of each state, given the states of its parent nodes [85]. BN based analysis of physical infrastructure performance is a growing field of research [86–89], as it provides an intuitive visualization of the problem in the form of a directed acyclic graph (DAG) allowing to reduce the complexity and interdependency between variables by logically shaping the network. In the context of seismic risk assessment, BNs have been applied to bridges [88] and buildings [86], or entire infrastructure systems [87] and for disaster management.

A number of studies report application of BNs to flood risk assessment. Sen et al. (2021b) [90] studied the resilience of housing infrastructure based on factors affecting recovery and reliability of the system. Urban flood disaster risk assessment using BN modelling is illustrated by Wu et al. (2019) [23] and Huang et al. (2021) [91] incorporating qualitative and quantitative variables and interfacing it with mapping software. BN can also be used for integrated index-based flood vulnerability assessment, where weights of system components are computed from various techniques and integrated using a BN approach [92]. Gehl and D'Ayala (2016) [93] have applied BN to assess multi-hazard vulnerability of road infrastructure considering scenarios of uncorrelated and cascading hazard

events including earthquakes, fluvial floods and associated ground failure.

This study presents the application of BN for the performance assessment of school systems in terms of disruption to education, when exposed to combined flood and seismic hazards. The objective is to estimate the disruption to education delivery due to reduction in structural and functional response of the buildings and to explore ways to reduce the disruption. The BN framework estimates the probability of different periods of disruption. The disruption may be caused by loss of school functionality from structural and non-structural damage inflicted by the hazards, or loss of accessibility to the school or change of function as shelters. The BN further integrate the social vulnerability with the duration of disruption, to study the influence of existing social vulnerability states on the expected disruption after an event. Finally, the study explores the mobility of students between schools with an aim to reduce the duration of disruption to education.

The methodology developed to study the sequential hazard effects on masonry school buildings and the application of BN for the performance assessment of the school systems is presented in Section 2. Section 3 provides the flood and seismic hazard characterisation of the case-study location, which informs the hazard inputs to the BN. Physical fragility functions derived from the sequential loading are a critical input for the BN. These functions for the representative buildings are generated through numerical analysis using an applied element method platform as presented in Section 4. Section 5 presents the BNs developed for the school system as defined in the methodology and Section 6- the results in terms of the duration of disruption to education and the influence of social vulnerability on the system.

2. Methodology

This study presents a BN based methodology to estimate the probability of the school system’s disruption in regions exposed to flooding and earthquake. The main factors affecting such probability can be broadly identified as: external causes determining accessibility to the site, functionality and physical vulnerability of the school infrastructure and social vulnerability of the population using the school system. A first essential step is therefore to estimate the physical fragility of the representative buildings under study, when exposed to sequential flood and seismic hazards. In order to determine the level and duration of disruption of school’s operations, a second important step is to determine the loss of school functionality, which also allows to harmonise the effects from different hazards. The third step is to link the influence of the community social vulnerability in determining the probability of system disruption.

Within the BN framework, the physical vulnerability of an asset type is represented by a set of fragility functions expressing the probability of occurrence of a damage state conditioned to the probability of occurrence of a given intensity of the natural hazard. Yearly recurring flooding, although may not cause major structural damage, produces saturation and material degradation in the masonry walls lower courses. Such degradation, usually not repaired, accumulates over the years. Therefore, if an earthquake of given intensity strikes in a region exposed to annual flooding, the damage caused is the result of the concurrent action of seismic acceleration,

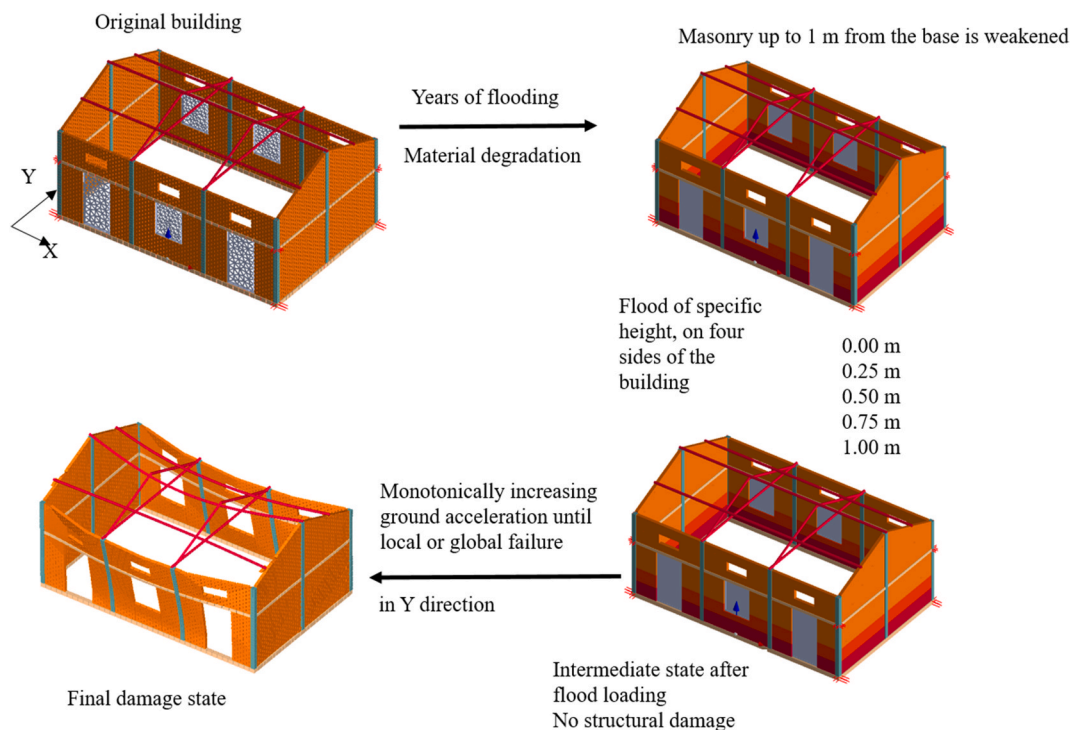


Fig. 1. Combined loading regime for flood and earthquake effects.

hydrostatic pressure from floodwater present at the time and the material degradation caused by previous flood events. In order to capture such effect in fragility functions, in this study a loading regime is devised that imposes, on the building with reduced material capacities in the lower courses, first a hydrostatic pressure representing the intensity of the flood hazard, followed by a static equivalent ground acceleration (GA) incrementally increased until structural failure occurs (Fig. 1). This process is explained in section 4.3. Henceforth, using a capacity spectrum approach, fragility functions are obtained for three damage states, following the methodology presented in Parammal Vatteri and D’Ayala (2021) [56]. A limitation of the loading regime is that it accounts only for the static loading from the flood inundation, and ignores any effects from flow velocity and debris impact and accumulation in this analysis. This reflects the observation that fluvial and pluvial flooding are often static in nature, with very low velocity [94], especially in floodplains. However, the analysis can be extended to consider these factors, following approaches available in literature (e.g. Refs. [95,96]).

The generation of these fragility functions, corresponding to five flood depths followed by seismic action, allows to define within the Bayesian analysis the probability of the state of damage of individual buildings, and therefore their loss of functionality, conditioned to the joint probability of a given Peak Ground Acceleration (PGA) and given flood depth. This in turns allows computing the probability distribution of the period of disruption of the school related to physical damage.

The Bayesian network structure, illustrated in Fig. 2, indicates the variables and their causal relationships, from which conditional probabilities for each of their possible states are computed, while the rationale and assumptions guiding these relationships between the system variables are explained in detail in Section 5. The *system* here represents a school infrastructure network formed by a number of school compounds in a locality. Schools are characterised by several buildings with different structural performance, housing different functions. The disruption due to schools’ physical functionality is then derived by correlating physical damage to function disruption. The states illustrating the period of disruption of the system are affected by loss of accessibility of the schools’ compound or loss of use as they are assigned as shelters. The network computes the probability of overall disruption states due to these factors when exposed to varying levels of the two hazards. The school population is characterised in terms of number of students and age, which together with their parents’ level of education and income determines the social vulnerability component. The network evaluates the modified system disruption, by considering the influence of social vulnerability on shelter-use besides a direct link to duration of inundation of the system. The latter accounts for the high probability of education interruption for student from socially vulnerable backgrounds, in the aftermath of disasters [15]. Although in this study, given the level of information available for the hazard a full georeferenced exercise is not possible, the BN is designed to allow to determine the influence of spatial correlation between school locations, community served, and floodwater depth distribution depending on local orography. The network design is discussed in greater detail in Section 5, where the variables, inter-dependency and observations from BN analysis are presented. The basic framework of Bayesian inference process adopted in this study is summarised in Appendix A.

The above two-step methodology, i.e. combined flood-seismic physical fragility assessment, followed by the BN-based system impact assessment, is illustrated through the case-study of school buildings in Guwahati city for which the hazard characterisation is presented in the next section.

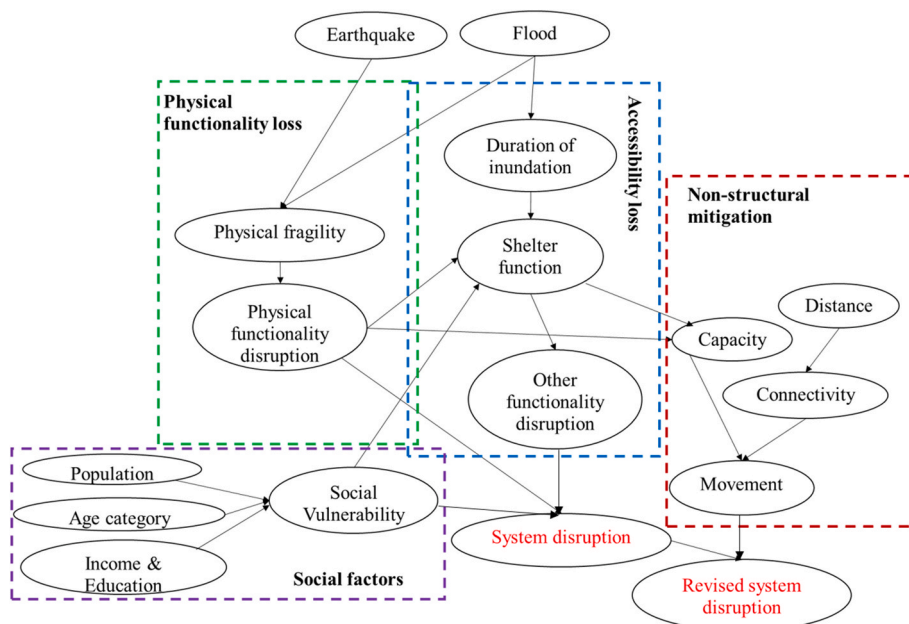


Fig. 2. Illustration of variables of the Bayesian Network and their relationship.

3. Hazards characterization in the case-study location

Assam is a highly flood prone state with over 40% of its land area vulnerable to flooding. Two major river systems - Brahmaputra and Barak and their valleys constitute the majority of the land area of the state [97]. Guwahati, the capital city of Assam, extends mainly along the south bank of the Brahmaputra River, over a total area of 262 km² known as the Guwahati Metropolitan Area, or Guwahati Urban Agglomeration. Within this, 216 km² fall under the Guwahati Municipal Corporation (GMC) area. GMC is divided into 31 administrative wards [98], whose boundaries are overlaid on a Google map [99] in Fig. 3.

Although floods are an annual phenomenon in Assam, the extent of damage caused by them has increased significantly in recent years [100]. Using satellite remote sensing datasets, the State Government and Disaster Management Authority (ASDMA) has classified its territory into five hazard classes, by frequency of flood inundation during a period of 10 years (1996–2015), ranging from very low (1–4 times) to very high (16–18 times). Accordingly, Guwahati city is ranked very low to low. However, other studies [101] focusing on the GMC's area, suggest that more than 50% of its territory is flood prone, of which 26.5% is chronically inundated, 22.7% occasionally inundated, 13.3% rarely inundated and 16.3% is inundation-free. Moreover, Sahoo and Sreeja (2017) [102] estimated that 26.78% of the GMC's area is under high flood hazard, based on a ranking scheme developed on the basis of flood depth and inundated area, as shown in Fig. 4.

Yearly floods in the city are characterised mainly as urban flash flood, originating from heavy monsoon rainfall (annual average of 1700 mm), concentrated over short period of time, causing congestion of drainage and inundation [103–105]. A second driver of flooding is recognised in the unplanned urbanisation, encroaching on natural wetlands and lakes and changing the land use patterns [106]. The natural drainage basins, affected by siltation and waste pollution, experience back flow from the rivers [107]. Some of the worst affected areas in the city, also characterised by high population density, are reported to witness 0.8–1.2 m water logging for a minimum of 3–4 days and a maximum of up to 20 days during heavy monsoons [103,105]. However, no statistical information on observed flood depth and frequency is provided in these studies.

Following the hazard map in Fig. 4, an in-depth study to develop flood inundation maps of Guwahati was conducted by Sahoo and Sreeja (2017) [102], that accounts for surface run off, topology and drainage network of the city. Urban Guwahati is divided into seven watersheds, with varying flood hazard intensities. Flood inundation depth and duration are computed for these watersheds for rainfall intensities of four return periods as shown in Table 1. The rainfall intensities are derived from available intensity-duration-frequency curves for the region, for a 15 min interval for each return period. They estimated a maximum inundation depth of around 1 m in the city for a 100 year rainfall event. Although more severe frequency is given in anecdotal evidence, this data is used in the present study for hazard characterization in terms of flood depth. As noted in Section 2, other flood hazard characteristics such as the flow velocity and impact loads from debris are not considered in this study.

With respect to seismic hazard, the Indian Standard 1893 [3] classification in Zone V suggests a MSK intensity of IX and above, and expected PGA of 0.18 g and 0.36 g for the Design Basis Earthquake (DBE) and the Maximum Considered Earthquake (MCE) (475 year and 2475 year return periods, respectively) [108]. Some in-depth studies suggest seismicity to the region much higher than the level assumed by IS 1893 [109–111]. This study adopts the hazard curves for Guwahati as proposed by Nath and Thingbaijam (2012) [109], which suggests PGA of 0.66 g and 1.36 g for DBE and MCE respectively, in order to consider the possibility of higher hazard intensity in

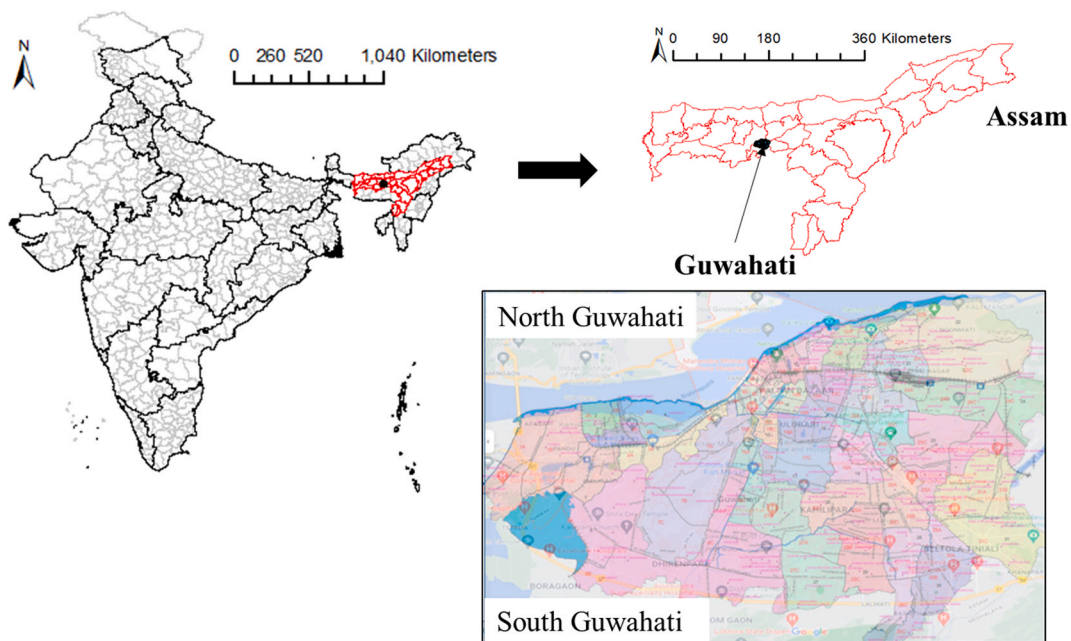


Fig. 3. Case-study location- Guwahati city (Guwahati Municipal Corporation Map from GMC (2021a) and Google map screen shot from Google Maps (2021).

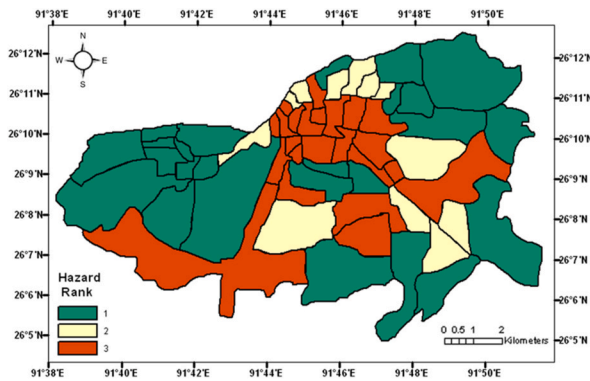


Fig. 4. Flood hazard zonation of Urban Guwahati: Sahoo and Sreeja, 2017 [102].

Rank 1: H1 and H2 less than 50% (Green)
 Rank 2: Either H1 or H2 more than 50% (Yellow)
 Rank 3: H1 and H2 more than 50% (Red)

where,

$$H1 = \frac{\text{Flooded area}}{\text{Total area of ward}} * 100$$

$$H2 = \frac{\text{Area with more than 0.2m flood depth}}{\text{Total area of ward}} * 100$$

Table 1

Estimated flood depth and duration at the case-study location [102].

Return period	Rainfall intensity (mm/h)	Area affected (km ²)	Worst case	
			Flood depth (m)	Flood Duration (h)
25 years	119.0	59.9	0.68	73
50 years	132.6	61.5	0.79	76
75 years	141.3	62.05	0.88	78
100 years	147.8	63.15	0.94	81

the region.

4. Physical vulnerability assessment

Physical vulnerability of schools, as identified in the introduction is one of the three key factors influencing the disruption of education. Numerical modelling provides a means for physical capacity and vulnerability assessment of the confined masonry schools under this study. Extreme Loading for Structures [112] - an Applied Element Method (AEM) based software, capable of performing advanced non-linear structural analysis, is used to perform the consecutive flood-seismic analysis of selected index buildings, i.e. buildings structures representative of the sample of schools surveyed in Guwahati (see section 1), chosen by applying a classification system presented in Parammal Vatteri and D’Ayala (2021) [56]. Of the masonry school buildings observed, 60% have flexible diaphragms, and variable level of confinement of the masonry panels by means of reinforced concrete elements, hence belong to the confined masonry typology as defined for the World Bank GLOSI library [25]. Three confined masonry index buildings (IB1, IB2, IB3, Fig. 5) with varying levels of seismic design, determined by the quality of connections, minimum available confinement and wall density, are chosen for the study, to understand the effect of their relative performance on the system resilience. IB1 has poor connections at the interfaces, minimum confinement in the form of plinth and lintel bands, corner columns and intermediate columns, resulting in *poor design level (PDL)*. IB2 is improved in respect to IB1, by good connections at the interfaces, resulting in *low design level (LDL)*. IB3 exhibits denser confinement, in the form of sill, roof and gable bands, besides good connections, resulting in *medium design level (MDL)*. Further details of the criteria defining the seismic design level are elaborated in Parammal Vatteri and D’Ayala (2021)

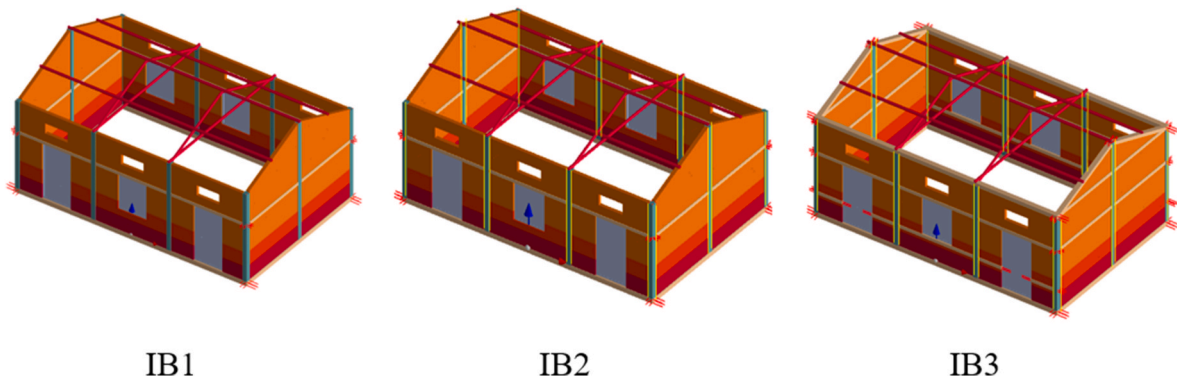


Fig. 5. Models of index buildings chosen for the study.

[56], which also lists other index buildings in the case-study database.

The ELS models are generated for a single structural unit from each IB, representing a classroom or office space, complete with shutters and roof trusses, simulating the flexible roof typology (Fig. 5). The models are built with the same geometry, in order to highlight the relevance of seismic design level on the lateral behaviour. The classroom blocks were formed of one or more of these units, however, the behaviour of the unit is considered representative of the block as the global response is limited by the absence of box-like behaviour, as further explained in the rest of the section. In the applied element method, the structure is discretised into the real configuration of a stretcher bond masonry wall, while concrete elements are meshed to compatible element sizes. Materials' characteristics, obtained from literature [113,114] are listed in Table 2. In the ELS analysis, failure is identified when partial or complete separation of portion of the walls are observed in the form of separation cracks, leading to a large increase in displacement. Failures can be local or global. Moreover, the integrity of the masonry can also be compromised by tensile strength being overcome and small "open cracks" being formed. The effect of recurring floods is simulated as reduction of masonry strength parameters in the lower 1 m of the walls, using as reference the floodwater depth identified in section 3.1. Following an experimental study on masonry infills in timber frames subjected to cycles of weathering and flooding [115], it is assumed that the lowermost 0.5 m and the next 0.5 m of masonry have 20% and 10% strength reduction with respect to the un-weathered masonry, respectively. Although the degradation can also be a function of the age of the structure, it is ignored in this study, since a full georeferenced spatial exercise of specific buildings is beyond the present scope, as noted in Section 2.

4.1. Flood-hydrostatic loading

ELS has in-built capability of applying distributed hydrostatic pressure by specifying the depth (h) and density (ρ) of water and the face on which it acts [112]. The loading scenario assumes that the buildings are surrounded by floodwater on all four sides, and there is no considerable ingress of water to the inside (Fig. 6a), as this assumption represents an extreme case of unbalanced lateral loading on the walls. The analysis considers incremental flood depths until a collapse mode is observed, identifying the critical flood depth for each IB. The results obtained for the three IBs are presented in Table 3. Failure of the buildings is caused in all cases by local failure of one of the more vulnerable wall panels with door as shown in Fig. 6b and c for IB2 with un-weathered and weathered material conditions, respectively. For the latter, it is evident that the damage is localised at the bottom of the walls and directly caused by the local deterioration of the materials.

The critical depth of water causing collapse varies by about 15% among the IBs, for the models with original material properties, while a reduction of up to 22% is observed for the weathered cases, compared to the non-weathered ones. The flood depth causing failure of the weakest confined masonry building, i.e. weathered IB1, is comparable to the results for unconfined masonry walls obtained by Kelman and Spence (2003) [57]. The values obtained are all greater than the maximum expected flood depth identified in section 3.1 for the case study area, therefore structural failure generated by flooding is not anticipated. However as localised cracking for lower water depths is observed, the reduction in material properties to repeated flooding is justified.

4.2. Seismic-ground acceleration loading

The seismic capacity of the three IBs is investigated using monotonously increasing Ground Acceleration (GA). This technique of applying GA for non-linear static pushover analysis overcomes the difficulty of such analysis on buildings with flexible diaphragms. Detailed description of the seismic analysis procedure, including failure mechanisms, definition of failure criteria and comparative performance are provided in Parammal Vatteri and D'Ayala (2021) [56]. The capacity curves for out-of-plane failure, the weakest failure mechanism, are shown in Fig. 7, for the IBs in their original condition and for material weathering. The seismic base shear capacity of the index buildings increases with increase in seismic design level, due to the better interaction between confinement and masonry walls. The material degradation does not have significant influence on the seismic capacity of IB1 and IB2, owing to their seismic-induced collapse being limited to the upper portions of the walls without mobilising the full strength of the lower courses. The ultimate capacity of IB3 is reduced by 10% in weathered material conditions, as in this case the full capacity of masonry walls is mobilised before the failure mode develops. It is noted that the study accounted only for moderate strength reduction in the lower 1 m of the masonry, which could also be a reason for this observation. Hence, the results could be improved by better characterization of strength reduction in masonry and concrete. However, the effect of the material degradation becomes evident when flood loading is also considered.

4.3. Sequential hydrostatic and seismic loading

The concurrent occurrence of a flood and seismic shaking is simulated by applying sequential loading to a weathered building, following the steps in Fig. 1. With reference to the 100 years maximum expected flood, the sequential loading is repeated for five increments of water depth, to derive the capacity curves associated to different probability of exceedance of water depth for this return

Table 2
Material properties of confined masonry used for numerical modelling.

Property	Value	Reference
Compressive strength of concrete	20 MPa	[116] minimum characteristic strength (f_{ck}) of concrete for RC construction
Young's modulus of concrete	22,360 MPa	[116]: $E = 5000\sqrt{f_{ck}}$
Compressive strength of masonry	4.63 MPa	[113,114]
Young's modulus of masonry	2546 MPa	[113]

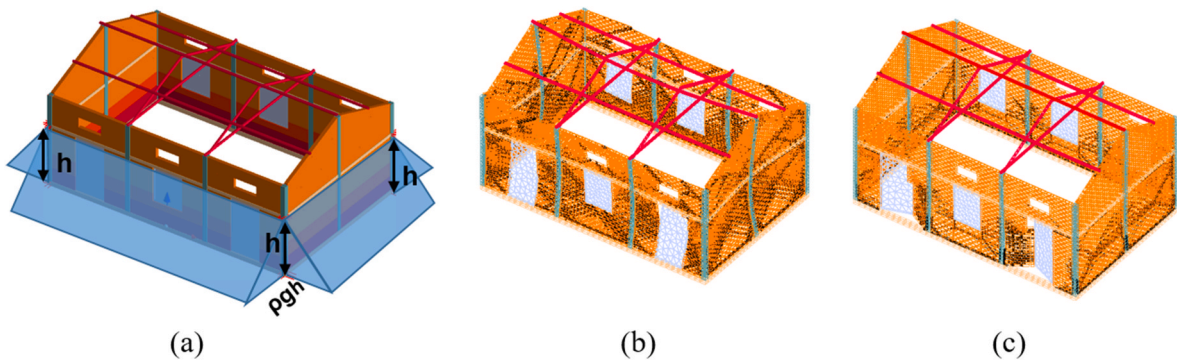


Fig. 6. a) Flood loading pattern on index buildings and crack pattern at failure for models with b) original material properties and c) weathered material properties.

Table 3
Capacity of the three IBs under hydrostatic flood loading- Lateral displacement of walls vs flood depth.

Typology	Critical flood depth causing collapse (m)	
	Original material properties	Weathered material properties
IB1	1.9	1.5
IB2	2.0	1.6
IB3	2.1	1.9

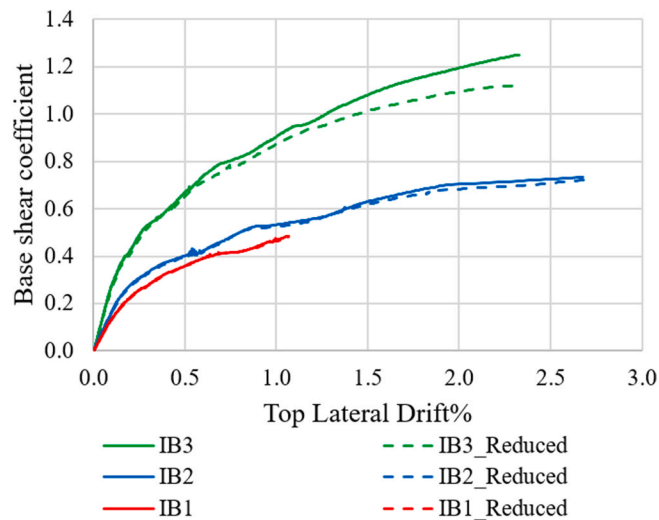


Fig. 7. Seismic capacity curves for three IBs with unweather and weathered material properties.

period. The ground acceleration is incrementally applied up to failure in the transverse (Y) direction, being the worst case (Parammal Vatteri and D’Ayala 2021) [56].

The combined loading condition has substantial impact on the response of the three IBs, which cannot be captured by the material degradation assumption, alone. Fig. 8 shows the capacity curves and the crack patterns at failure for the worst case of flood (1 m) combined with the seismic action. The capacity curves show reduction of strength capacity up to a maximum 17.5%, 9% and 26% for the IB1, IB2 and IB3 respectively (Table 4). IB3’s displacement capacity is particularly affected with a decrease of 36% for 1 m flooding (Fig. 9 and Fig. 10). An appreciable reduction in stiffness for IB1 and in ductility for IB3 are also noticeable. The additional confinement present in IB3, while improving its strength capacity by 35%, introduces a discontinuity at sill level, causing localised failure, which affects global ductility by up to 40%, as compared to IB2.

The 1 m depth flood followed by ground acceleration defines a step change in the behaviour of the three IBs, with reduction of 42%, 25% and 16% in the initial stiffness, for IB1, IB2 and IB3 respectively. However, in the case of IB1 and IB2, localised failure modes are highly influenced by the construction geometry, and the lack of a sill tie beam, whereby lower ultimate drift can be observed for 0.75 m flood depth (Table 4, Fig. 9a and b). The sill tie beam in IB3 (Fig. 9c) provides sufficient restraint to the central panel to prevent the base course from failing, while the lateral panels’ failure is localised and does not affect the overall base shear capacity which is ensured

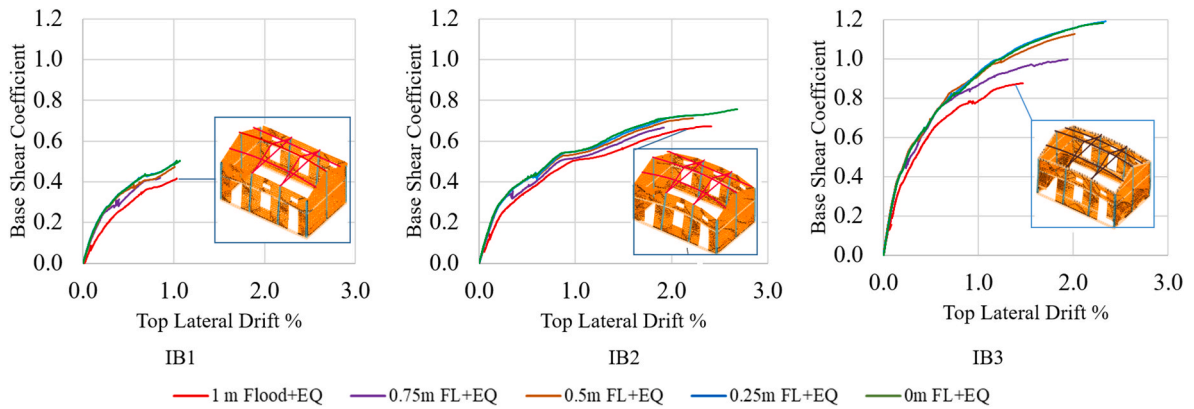


Fig. 8. Capacity curves for out-of-plane failure of three IBs after combined loading.

Table 4
Capacity curve parameters for three IBs under sequential flood and seismic loading.

	Flood depth (m)	Yield BSC	Yield drift (%)	Change in yield BSC (%)	Change in yield drift (%)	Ultimate BSC	Ultimate top drift (%)	Change in ultimate BSC (%)	Change in ultimate drift (%)
IB1	0.00	0.30	0.23	–	–	0.50	1.07	–	–
	0.25	0.28	0.21	4.69	8.95	0.50	1.02	1.57	4.18
	0.50	0.27	0.21	7.81	7.74	0.47	1.01	5.93	5.36
	0.75	0.26	0.22	10.94	5.55	0.42	0.85	16.73	20.54
	1.00	0.26	0.35	12.50	–51.33	0.42	1.04	17.48	3.17
IB2	0.00	0.46	0.32	–	–	0.73	2.29	–	–
	0.25	0.43	0.29	7.00	7.38	0.73	2.29	0.06	0.08
	0.50	0.41	0.27	12.00	15.83	0.71	2.22	2.32	2.98
	0.75	0.35	0.23	24.00	26.11	0.67	1.92	8.53	16.11
	1.00	0.35	0.32	25.00	0.38	0.65	2.05	10.57	10.63
IB3	0.00	0.78	0.38	–	–	1.18	2.31	–	–
	0.25	0.78	0.37	0.00	0.79	1.18	2.24	0.03	3.18
	0.50	0.74	0.33	5.36	11.73	1.11	1.90	5.88	17.95
	0.75	0.72	0.33	7.74	11.74	0.99	1.73	16.78	25.29
	1.00	0.66	0.38	15.48	–0.92	0.88	1.47	25.94	36.46

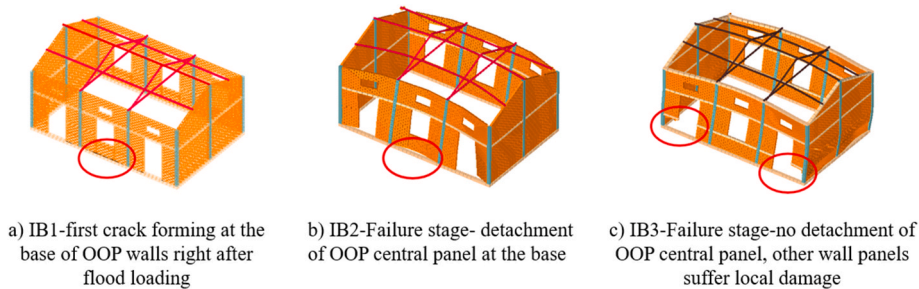


Fig. 9. Behaviour of three IBs at different load stages under the load case of 0.75 m flood followed by seismic action.

through the confining columns and transfer of loading to the gable walls.

To define fragility functions for different damage states, three damage state thresholds are visualised in Fig. 10, for IB3. Cracking initiates in the out-of-plane piers and at the bottom of all walls at point A. Cracks then propagate to spandrels of the OOP walls and diagonal cracks start appearing in the in-plane gable walls at point B. Even though the OOP walls suffer local separation of masonry elements at the bottom of the wall, the building withstands further lateral load while maintaining stability until the point C, beyond which large deformations occur for small increment of loads. At this point, the cracks are spread all over the OOP walls and the lower portion of IP walls, although continuous cracks are limited by the presence of RC confining elements. The effect of flood loading and weathering on ultimate collapse, beyond point C is highlighted for IB3 in Fig. 11. The gable walls show larger deformation and damage in the weathered model, whereas in the un-weathered model, they act as compression struts until ultimate failure of the building. The base shear sustained by the un-weathered model at ultimate collapse is about 1.6 times that of the weathered and flood-affected model.

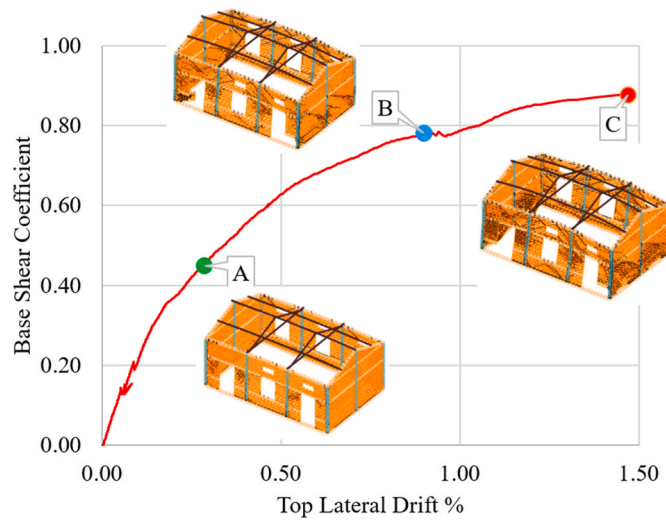


Fig. 10. Damage progression in IB3 for combined 1 m flooding and incremental seismic action.

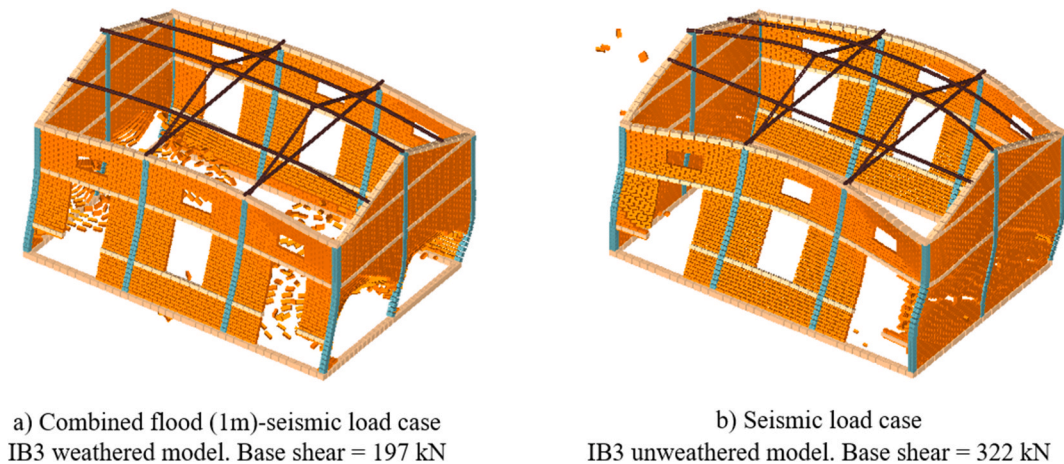


Fig. 11. Comparison of collapse failure modes at an advanced stage for IB3 with and without material degradation due to flooding and 1 m flood depth hydrostatic load.

4.4. Fragility assessment

The capacity curves obtained after sequential hydrostatic and ground acceleration loading, depicted in Fig. 8, are idealised to bilinear curves and fragility curves are derived using PGA as seismic intensity measure (IM). Details of the procedure for the application of N2 method [117] using a suite of ground motions from FEMA_P695 (2009) [118] for this class of IBs are presented in Parammal Vatteri and D'Ayala (2021). The three representative points A, B and C, shown in Fig. 11, correspond to the thresholds of Immediate Occupancy (IO), Life Safety (LS) and Collapse Prevention (CP), damage states, used for the derivation of fragility curves. The results are presented in Fig. 12 and the fragility parameters are listed in Table 5.

The fragility functions clearly capture the improvement in performance from IB1 to IB3 due to better seismic design level, in all combinations of flood depth and seismic loading. It should be noted that the reduction in displacement capacity observed for IB2 in relation to lower flood depths, is reflected in the fragility functions at both IO level, and LS level, compounded with larger dispersion compared to the other two IBs. This novel combined analysis process thus enables probabilistic assessment of the school systems across the intensity ranges of both hazards, illustrating its ability to capture physical effects in multi-hazard scenarios. This suite of fragility functions is used as input to the Bayesian Network in the following section, to represent the probabilistic distribution of the physical performance of the IBs.

5. BN for combined flood and seismic vulnerability assessment

A network of multiple schools in a region or city forms its school infrastructure, providing the crucial service of education to the community inhabiting it. As a collection of structural and non-structural components interlinked to provide the common objective of

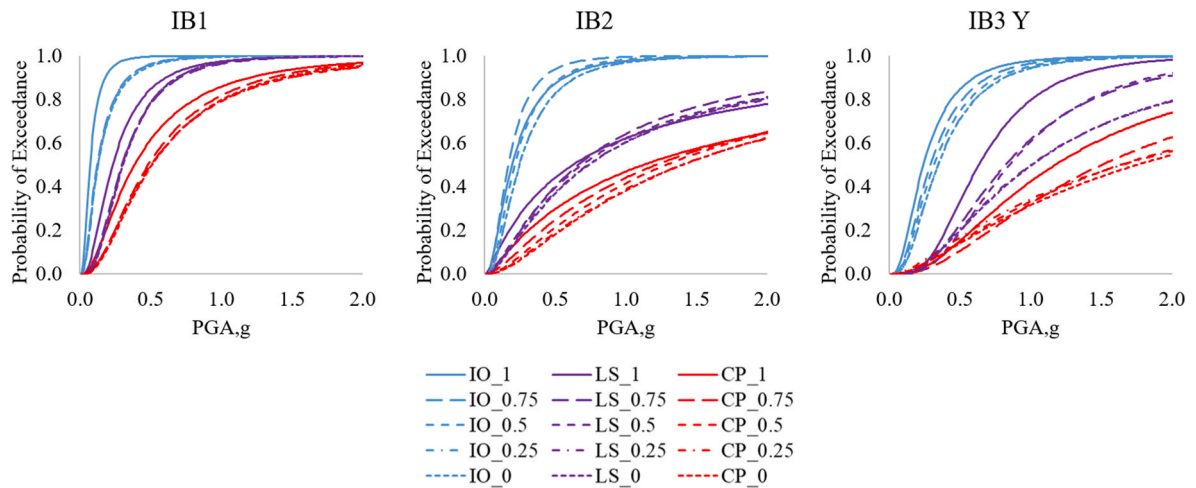


Fig. 12. Fragility curves for sequential loading scenario for three IBs.

Table 5
Fragility parameters.

Performance levels	Median PGA of fragility curves corresponding to Flood depths (m)					Range of dispersion β
	1	0.75	0.5	0.25	0	
IB1						
IO	0.070	0.123	0.128	0.128	0.128	0.732–0.815
LS	0.231	0.297	0.301	0.301	0.305	0.633–0.754
CP	0.385	0.483	0.503	0.503	0.510	0.804–0.888
IB2						
IO	0.193	0.167	0.212	0.245	0.247	0.708–0.835
LS	0.625	0.663	0.690	0.730	0.737	1.127–1.515
CP	1.124	1.212	1.285	1.396	1.401	1.131–1.526
IB3						
IO	0.242	0.291	0.316	0.344	0.345	0.672–0.711
LS	0.635	0.823	0.851	1.001	1.010	0.549–0.858
CP	1.175	1.505	1.639	1.647	1.753	0.830–1.236

delivering education, school infrastructure can be considered as a system [119], for which natural hazards are the external factors producing changes in performance and risk of failure. A generic BN for a school infrastructure network having n schools is developed to study the impact of combined hazards on the school system in terms of disruption to education as shown in Fig. 13. The BN is subdivided in four parts, reflecting the different nature and domain of the variables considered as contributing to the overall disruption to the system, as already discussed in Section 2. Table 6 presents the variables' name, symbol, and their assigned states.

The two root nodes, EQ and FL represent the earthquake and flood hazard respectively, which can be input as discretised hazard curves providing probability distribution of hazard in terms of PGA for earthquake and inundation depth for flood, in this study obtained by Nath and Thingbaijam (2012) [109] and Sahoo and Sreeja (2008) [102] respectively. The characteristics of such distributions shall depend on the seismicity and flood susceptibility of the location under study. As the exact location and topography of the schools' compounds is not available, the assumption is that all compounds are exposed to the same value of intensity attributed to each hazard. Variability in accessibility to schools is incorporated through the assumed probability of flooding at the school site and the basin within which the school is located. These features can be fine-tuned for a more specific case study, where school location is available. The two hazard events are considered independent of each other, and hence, the joint probability of exceeding a given inundation depth and PGA is estimated by direct multiplication of the two event probabilities, while performing operations on the network (see Equation A.4 in Appendix A for an illustrative example). EQ and FL directly link into various states of loss of schools' physical functionality (PF_i), as grouped within the green box in Fig. 13. This expands to a first sub-BN, Part A, involving fragility curves for different building typologies under combined loading scenarios, functionality loss of buildings (BF_i) and outputs physical functionality (PF_i), leading to the system's disruption due to physical functionality state (T_{PF}). More detail on Part A is provided in section 5.1.

As seen in section 3, yearly flood events may last days or weeks, but it might take schools many weeks or months to resume full operations. Earthquakes might last seconds or few minutes, but it might take months or years to repair and reconstruct [120]. Part B (blue box in Fig. 13 further detailed in section 5.2) estimates the duration of disruption in scenarios where schools fail to deliver

Table 6
Expansion of Variables in the Bayesian network shown in Fig. 13.

Part of the network	Variable abbreviation and expansion
Part A	EQ-Earthquake FL-Flood depth
Part B	PF _i : Individual school's physical functionality disruption D _f -Duration of flooding at school site D _B - Duration of flooding in the basin SH _i -Shelter function of school
Part C	OF _i - Other (non-structural) functionality disruption at individual schools P _i -Population C _i : Category of school IE-Income and Education of Parents SV _i -Social vulnerability of individual schools
Part D	DS _{i,j} : Distance between any two pair of schools i and j SZ _i : Size of school CN _{i,j} : Connectivity between schools i and j CP _i : Capacity to accommodate moving students M _{i,j} : Movement between schools i and j
Overall System	T _{OF, Ri} : Revised duration of disruption of individual schools T _{PF} -Duration of disruption due to school system's physical functionality loss T _{OF} -Duration of disruption due to other (non-structural) functionality loss T _{OF, R} : Revised duration of non-structural disruption of school system T _{SYS} -Overall duration of disruption to school system T _{SYS, R} -Revised overall duration of disruption to school system SV -Social vulnerability of the system T _{SYS, SV} -Overall disruption to education, considering the social vulnerability T _{SYS, SVR} -Revised overall disruption to education, considering the social vulnerability

and their comparison with the original T_{SYS} and $T_{SYS,SV}$ before considering the mitigation.

Part D of the network (shown in red box in Fig. 13 and discussed in section 5.5) explores the possibility of mobility of students between schools as a mitigating measure to reduce the overall duration of disruption to education. Options such as double-shifts can be viable to mitigate education loss [84] and explore the benefit of the system dimension of the school infrastructure. The assumption is that by moving students from a school that is non-functional, to a nearby functional school, the overall disruption to the school infrastructure system, and hence to the education delivery is reduced. For the sake of this analysis, it is assumed that the administrative system allows this temporary mobility and even encourages collaboration between neighbouring schools at times of emergency. The goal is therefore to compute the probabilities of 'revised downtime states' of each school when mobility is included. If mobility is not possible due to any of the conditions set out for the network, it means that the school infrastructure system is vulnerable and has no redundancy.

To obtain the revised period of disruption ($T_{OF, Ri}$) after allowing mobility, the following factors are considered in Part D: category of school with respect to age of students (C_i), distance between schools ($DS_{i,j}$) and size of schools (SZ_i). The first two parameters determine the connectivity of schools ($CN_{i,j}$) while the last factor contribute to the capacity of the schools (CP_i) to allow movement ($M_{i,j}$) of students. For DS and CN , the combination is considered irrespective of the direction of movement of students, i.e. $DS_{i,j}$ means distance between schools i and j , which is the same as $DS_{j,i}$. Hence, there will be $C(n, 2)$ combinations of $DS_{i,j}$ and $CN_{i,j}$ in a network of n schools. The direction is important for the M node, describing the movement of students, as $M_{i,j}$ denotes mobility of students from school i to j , and $M_{j,i}$ in the opposite direction. These are not the same, as the physical and functional conditions of each school-pair are considered for the calculation of conditional probability of these nodes. Hence, there will be $P(n,2)$ permutations of M nodes in the network of n schools.

The following subsections detail the CPT definitions of each part of the network and the overall system. The complete network in Fig. 13 contains 24 variables, 15 of which appear in sets dependent on the number of schools in the system. The total number of nodes N in the BN for n schools is,

$$N = 11n + 2 * C(n, 2) + 1 * P(n, 2) + 10 \tag{1}$$

One advantage of this network structure is that can be adapted to represent n clusters of schools, by simply inserting properties of cluster for each nodes instead of individual schools, in which case, the analysis can be carried out at the larger scale of the school infrastructure of the whole city. The scalability is especially useful, considering that the typology of buildings and hazard effects could be similar within a small locality having a cluster of schools, while varying considerably from locality to locality. For instance, the school buildings observed in the northern area of Guwahati city were predominantly old, single story masonry or CM buildings, while the more urbanised areas in south Guwahati housed RC school buildings as well (see Ref. [56]). The framework developed in this study would allow to analyse clusters and determine the spatial variance in vulnerability and resilience of the school infrastructure across a metropolitan urban area such as Guwahati.

5.1. Part A - the sub-BN for disruption due to school's physical functionality (PF_i) level

Each school compound comprises multiple building blocks of different construction typology, hosting single or multiple functions,

such as classroom, office, refectory, etc., and it can therefore be considered as a sub-system within the school infrastructure system. A specific BN is generated to estimate the functionality of each school compound and of a system of three compounds as shown in Fig. 14. Variables used in this part of the network are detailed in Table 7 with their assigned states. From the survey of 86 schools in the case study area [122], it results that more than 75% had two buildings in the compound. Hence, each school in this network is assumed to have two building blocks, B_{i1} and B_{i2} , where i represent the serial number of the school, while 1 and 2 identify the building block, each being assigned any one of the three IB typologies, introduced in Section 4, with the corresponding fragility functions derived in Section 4.3. Each B_{ij} node has four states, as shown in Table 7. Therefore, the CPTs of each B_{ij} node has 400 columns, corresponding to 20 EQ states, 5 FL states and 4 performance states. Each entry of the CPT corresponds to one combination of these parents' and its own states. The two blocks together provide three basic 'building functions' of the school, i.e. classroom, office and refectory, denoted as BF_{i1} , BF_{i2} and BF_{i3} . These nodes are given three states (Table 7). The CPTs of BF_i nodes are derived with respect to the fragility state of the building/s hosting that function: i) no damage and immediate occupancy correspond to unaffected functionality, ii) collapse prevention correspond to functionality total loss, iii) all other combinations of fragility states correspond to partially functional. The nodes PF_i , represents the physical functionality of the school as a system, assuming three possible states of disruption, conditional to the states of BF_i nodes as shown in Table 8. The inferred probabilities for each state of the PF_i nodes are carried forward to Part B of the network, to assess the suitability of using the school as a shelter.

The performance of Part A subsystem, is given by node T_{PF} , measuring the disruption to its physical functionality in terms of duration of recovery, whose CPT is obtained by combining the probabilities of individual school functionality states. Of the three possible states, if the damage level is beyond immediate occupancy, but not reaching life safety, it is expected to cause up to 3–4 months of recovery time, translating to a system performance state of 'partially functioning'. Such a recovery period implies options of rapid repair and rehabilitation such as the ferrocement technique [32]. Physical damage corresponding to the life safety threshold would require major structural repair, and 1 year is considered as a reasonable period. The T_{PF} node is an input to the overall system disruption period ' T_{SYS} ', as shown in Fig. 13.

5.2. Part B: disruption from other causes

Part B evaluates the probability of different states of duration of disruption to education for individual schools from other causes of functionality loss (OF_i), i.e. other than the functionality loss induced by physical damage. These include the lack of accessibility due to inundation at the site of school and its basin, or the change in use, from educational to shelter or other post event function. Variables in this part of the network and their states are listed in Table 9. The CPTs of duration of inundation at the school site (D_i) are derived from the flood depth hazard states, defined in number of days as per evidence provided by Sahoo and Sreeja (2008), in absence of systematic spatial data on flood depth and duration across the case-study location. Four states are assigned to D_i , linked to the five states of flood depth given by the hazard curve. The duration of inundation in the basin (DB_i), also linked to flood depth, is defined in weeks rather than days as per evidence provided by Chakraborty and Singh (2016) [103]. D_i and DB_i allow to differentiate the accessibility of the school site from the state of inundation of the community, reflecting diverse topographic and hydrological features of the area under study. The state of these two variables determine the possible state of the school-shelter.

The SH_i has four states, ranging from 'not used as a shelter' to 'used as shelter up to four months' (Table 9). Besides D_i and DB_i , the

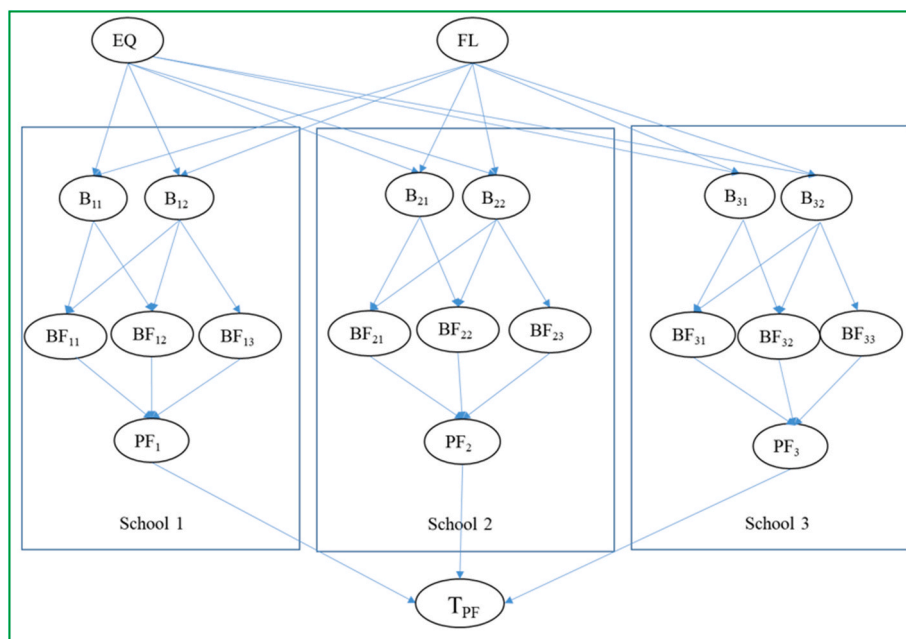


Fig. 14. BN for Part A: School functionality network.

Table 7
Variables and their states in Part A of the Network.

Variables	States
EQ-Earthquake	20 PGA states and their annual exceedance probabilities as defined by the earthquake hazard curve (see Appendix B).
FL-Flood depth	5 flood depth values and their annual exceedance probabilities derived from Ref. [102] (see Appendix B).
B_i - Physical fragility of individual buildings	<ol style="list-style-type: none"> 1. No damage 2. Immediate Occupancy (IO) 3. Life Safety (LS) 4. Collapse Prevention (CP)
BF_i - Building Functionality	<ol style="list-style-type: none"> 1. Function is unaffected 2. Partially functional 3. Non-functional
PF_i : Individual school's physical functionality, with assumed recovery period	<ol style="list-style-type: none"> 1. Intact: minimal disruption, under 1 week 2. Partially functioning: up to 3 months 3. Shutdown: 1 year
T_{PF} : Duration of disruption due to physical functionality loss of the school infrastructure system	<ol style="list-style-type: none"> 1. Short functionality loss under 1 week and minimal disruption 2. Medium functionality loss up to 3 months 3. Long functionality loss up to 12 months

Table 8
Conversion of functionality state to individual school functionality state.

Building Functionality state (node BF_i)	Physical Functionality state (node PF_i)
All BF_{i1} , BF_{i2} & BF_{i3} are in fully functional state (state 1)	Intact (1)
All BF_{i1} , BF_{i2} & BF_{i3} are in shutdown state (state 3)	Shutdown (3)
All other combinations	Partially functional (2)

Table 9
States of variables in Part B of the network.

Variable	States
D_i -Duration of flooding at school site	<ol style="list-style-type: none"> 1: No inundation 2: 1–2 days 3: 3–6 days 4: 7–10 days
DB_i - Duration of flooding in the basin	<ol style="list-style-type: none"> 1: No inundation in basin 2: Inundation up to 1–2 weeks 3: Inundation up to 3–4 weeks
SV_i -Social vulnerability of individual schools	<ol style="list-style-type: none"> 1: Low vulnerability 2: Medium vulnerability 3: High vulnerability
SH_i -Shelter function of school	<ol style="list-style-type: none"> 1: Not used as shelter 2: Used as shelter for up to 2–3 weeks 3: Used as shelter for up to 1–2 month 4: Used as shelter for up to 3–4 month (longer recovery)
OF_i - Duration of disruption at individual schools from other functionality losses	<ol style="list-style-type: none"> 1: Negligible: under 1 week 2: Disruption for 2–3 weeks 3: Disruption for 1–3 months 4: Disruption for 4–12 months
T_{OF} - Duration of disruption of school infrastructure system from other functionality loss	<ol style="list-style-type: none"> 1: Short: 'Low' disruption up to 3 weeks 2: Medium: 'Medium' disruption up to 3 months 3: Long: 'High' disruption up to 12 months

other two parent nodes determining SH_i states are the school functionality PF_i and the state of social vulnerability of the community SV_i . For instance, the school is more likely to be used as a shelter if the basin is inundated, but the location of school is not, owing to its high altitude or better drainage system, and if its functionality from PART A is satisfactory. A high state of social vulnerability also increases the probability of the school being used as a shelter for extended period, while the community recovers. Table 10 provides the CPT of possible states of SH_i as a function of the states of its parent variables. Uniform probability distribution applies to all states.

The CPT of individual school's disruption period from other functionality loss (OF_i) therefore is derived considering the correlation between duration of inundation at school site and shelter function of schools. Four possible states are defined for the disruption period (see Table 9) considering the following possible combinations of the parent nodes states:

Table 10
CPT for SH node, conditioned on states of PF_i , D_i , DB_i and SV_i (corresponding states of the variable in brackets).

PF_i	D_i	DB_i	SV_i	SH_i state	Combination rule
shutdown (3)	more than 2 days of inundation at school site (3,4)			not used as a shelter (1)	OR
intact or partially functional (1,2)	less than 2 days of inundation at school site (1,2)	inundation up to 2 weeks in basin (2)	Low or medium level High level	used as shelter up to 3 weeks (2) used as shelter up to 2 months (3)	AND
intact or partially functional (1,2)	less than 2 days of inundation at school site (1,2)	inundation up to 4 weeks in basin (3)	Low or medium level High level	used as shelter for up to 2 months (3) used as shelter for up to 4 months (4)	AND

- The school not being used as a shelter and inundation at site being minimum (D_i state 1 or 2), the non-structural disruption is under one week (OF_i state 1).
- The school’s SH_i has the longest duration (up to 4 months) leads to a disruption period of up to 12 months (OF_i state 4), irrespective of the inundation at site.
- Other combinations of D_i and SH_i states lead to duration of disruption of 2–3 weeks or 1–3 months.

The overall disruption time T_{OF} for the school from non-structural causes is then defined applying combination rules, such that, the condition of all schools under 3 weeks of disruption is considered to cause an overall ‘short’ disruption of the education system. All schools up to a maximum of 3 months disruption leads to a ‘medium’ disruption of the system, while all other combinations lead to ‘long’ disruption, as at least one school will be facing 4–12 months of disruption individually.

5.3. Part C: Social vulnerability

For each individual school, the social vulnerability component is determined by the size of student population (P_i), representing the exposure factor, and the category of school (C_i) based on the age group of students, which relates directly to their vulnerability in a hazard event. Three states and their probabilities are assigned for each of these nodes based on the statistics of schools surveyed (Table 11).

The social vulnerability of the community, is accounted via the combined income and education (IE) of the parents of students in the area, for which three possible states and associated probabilities (Table 11) are based on the 2011 census of India, which estimates a literacy rate of 73.18%, and a proportion of the population below the poverty line of 34% for Assam [123–125]. Given the poor resolution of this indicator, IE is assumed as common value to all schools in one locality. The CPT of SV_i are defined considering the P_i and C_i states of individual schools, and the common IE state of the community, following the assumption that the larger the school population and the lower the children age attending a school compound, the higher the social vulnerability of the individual school’s student population, amplified by poorer state of income and education of the community. Therefore:

1. Highest population or lowest age category when combined with the poorest income-education state lead to *high* SV_i ;
2. When P_i and IE are either 1 or 2 and C_i is either 2 or 3 (see Table 11) indicating low vulnerable conditions, the SV_i state is *low*;
3. All other combinations lead to a state of *medium* social vulnerability.

The social vulnerability of individual schools contributes to the level of social vulnerability of the overall school network (SV). The CPTs of the overall system’s social vulnerability states are defined by the combination of multiple schools being in any given state.

Table 11
Variables and their states in Part C of the Network. Assigned probabilities of root nodes are given in brackets.

Variables	States	Assigned Probabilities of root node states
P_i -Population	1: 0–50 students 2: 50–100 students 3: >100 students	0.1: Based on survey statistics 0.3 0.6
C_i : Category of school	1: LP school: class 1 to 5 2: ME school: class 6-8 3: HS school: class 9-10	0.56: Based on survey statistics 0.22 0.22
IE -Income and Education of Parents	1: Above average 2: Average 3: Below average	0.3: Based on 2011 census data 0.4 0.3
SV_i -Social vulnerability for individual schools	1: Low vulnerability 2: Medium vulnerability 3: High vulnerability	
SV -Social vulnerability of the system.	1-Low vulnerability 2-Medium vulnerability 2-High vulnerability	

5.4. Overall duration of disruption of the school system

The ‘impact’ of combined hazards on the school system and the delivery of the education can be quantified as the *Overall Duration of Disruption* to the education system (T_{SYS}) (Fig. 13) which is obtained as the combined product of the conditional probabilities of disruption due to schools’ physical functionality (part A- T_{PF}) and other functionality losses (part B- T_{OF}). T_{SYS} is then modified by the level of social vulnerability (Part C) providing a *Modified Probability of Duration of Disruption*, $T_{SYS,SV}$. Both T_{SYS} and $T_{SYS,SV}$ have three states, *short*, *medium* and *long* disruption. The CPT of T_{SYS} is defined with the following criteria:

- For the overall system to receive *short disruption* both parents should be in *short disruption* state, i.e. T_{PF} is within 1 week and T_{OF} is limited to *under 3 weeks*.
- On the other hand, T_{SYS} will receive *long disruption*, hence *high impact*, if either of the two parent nodes are in *long disruption* state, i.e. T_{PF} or T_{OF} is up to a year.
- In all other combinations, the overall system is in *medium disruption or impact* state, up to 3 months.

CPT of $T_{SYS,SV}$ is defined by considering the observation that children from highly vulnerable communities are more likely to miss schooling even when other physical and functional aspects of schools are undisturbed or brought back to normal after an event. To incorporate this into the BN, CPT of $T_{SYS,SV}$ assumes that the state of overall disruption, T_{SYS} , increases from *short* to *medium* and *medium* to *long*, if the SV state is ‘*high*’. Implications of ‘*low*’ SV state to possibly reduce the long disruption period from other physical and functional causes is not explored in this analysis, due to lack of evidence to quantify this link.

5.5. Part D: Students’ mobility effect on duration of disruption of the system

Part D of the network applies the conditions that allow mobility of students between schools within the school infrastructure system to estimate a revised non-structural disruption duration of the system $T_{OF,R}$ in order to improve the probability of short disruption as originally estimated through the T_{OF} node. The mobility variable $M_{i,j}$ between any two schools is decided based on connectivity between two schools, capacity of accommodating students and shelter function of individual schools. Table 12 shows the states of variables in this part of the network. The receptive capacity (CP_i) of schools is dependent on the functionality of individual schools (PF_i) in addition to their size (SZ_i) to accommodate more students, moving from nearby schools. The root nodes C_i and SZ_i are defined by three states, while $DS_{i,j}$ is a binary node as given in Table 12. Their probabilities are assigned based on the statistics of the sample of schools surveyed in the locality. Similar to part B of the network, logical conditions are applied between the states of C_i , $DS_{i,j}$ and PF_i and SZ_i to derive the CPT of $CN_{i,j}$ and CP_i , respectively as the following: 1) with youngest age category of students, $CN_{i,j}$ is possible if the $DS_{i,j}$ is less than 1 km, while for other age categories the $DS_{i,j}$ is irrelevant. 2) PF_i state of ‘*intact*’ and SZ_i state above ‘*small*’ indicate a positive state of CP_i , while other combinations of PF_i and SZ_i lead to its negative state.

Two states are defined for the mobility node $M_{i,j}$ corresponding to positive and negative possibility of re-allocation of students, as defined in Table 13 for any couple of schools. $M_{i,j}$ is conditional to connectivity ($CN_{i,j}$), to the receptive school capacity and to its function not being shelter.

The CPT of revised disruption period of individual schools, $T_{OF,Ri}$, is defined for a system with three schools as shown in Table 14, assuming that if mobility is possible from school i to any other school in the network, the disruption of this school reduces to ‘*negligible*’ disruption state, as students can be educated in other schools during its recovery. The revised disruption state of the overall system, $T_{OF,R}$, is then computed using the same model as Part B, updated with the new disruption periods.

Section 6 presents the results of the analysis for a system of three schools, which contains 56 nodes. On an Intel(R) Core(TM) i7-7600U CPU @ 2.80 GHz 2.90 GHz with 16 GB RAM, it takes under 70 s to run this network. As mentioned in Appendix A, the network

Table 12
Variables and their states in Part D of the network. Root nodes are written in italics and their assigned probabilities are given in brackets.

Variables	States	Assigned Probabilities of root node states
$DS_{i,j}$: Distance between any two pair of schools i and j	1: Close, less than 1 km 2: Far, more than 1 km	0.43 0.57 Based on a sample data
SZ_i : Size of school	1: Large, more space than present population 2: Adequate, good enough for current population 3: Small, barely sufficient for current population	0.33 0.33 0.33 Assigned uniform probabilities
$CN_{i,j}$: Connectivity between schools i and j	1: Yes, if walkable ($DS_{i,j} = 1$ and $C_i = 1$) or $C_i > 1$ 2: No, if not walkable	
CP_i : Capacity to accommodate moving students	1: Yes 2: No	
$M_{i,j}$: Movement between schools i and j	1-Yes 2-No	
$T_{OF,Ri}$: Revised duration of disruption of individual schools	1-negligible 2-short 3-medium 4-long	
$T_{OF,R}$: Revised duration of disruption of school infrastructure system	1-short 2-medium 3-long	

Table 13
Conditions for defining CPT of $M_{i,j}$.

SH_j	CP_j	$CN_{i,j}$	$M_{i,j}$ state	Combination rule
–	–	No (2)	No	OR
No(1)	Yes (1)	Yes (1)	Yes	AND
All other combinations			No	–

Table 14
Conditions for defining CPT of $T_{OF,Ri}$.

$M_{i,j}$	$M_{i,k}$	OF_i	$T_{OF,Ri}$ state	Combination rule
Yes(1)	Yes(1)	–	Negligible(1)	OR
All other cases		1,2,3,4	Same as T_i state	–

was first moralised, then triangulated to identify the elimination order, following which 38 cliques are formed to create the junction tree, in the Bayes Net Tool in order to carry out Bayesian inference.

It is to be noted that by increasing the number of schools in the system, the size of the network increases as per Eq. (1), requiring higher computational effort for a realistic system of schools or clusters of schools. The network design shown in Fig. 13 is the most straightforward or ‘naïve’ way of connecting all system variables in a converging manner to produce a final system performance output. For very large systems, special techniques such as minimum link sets or minimum cut sets may be identified to divide the system into a combination of parallel or series subsystems, to manage the computational load [89].

6. Results and discussion

The Bayesian network illustrated in section 5 is applied to a system of three schools with the following simplifying assumptions: the analysis considers only one IB type - IB2 -, for the general discussion on the probability and duration of disruption to the system, while the sensitivity to typology is presented separately. Without loss of generality, identical prior probabilities and CPTs are assigned to variables across schools, such as P_b , C_b , $DS_{i,j}$ etc., effectively assuming the same condition for all the schools. The same applies for the variable IE .

Herein the results are presented in terms of the probability of disruption states for 1) the overall system disruption due to physical and other (non-structural) functionality loss, T_{SYS} ; 2) the modified overall system disruption due to the community social vulnerability, $T_{SYS,SV}$ and 3) the reduced overall system disruption $T_{OF,R}$ due to the mobility of student between schools. Three states of these variables short, medium and long duration of disruption, namely DD_s , DD_m and DD_l respectively, are considered. Furthermore, the influence of parent nodes on the system disruption states is assessed by means of a sensitivity study using the one-at-a-time (OAT) approach and by defining possible realistic scenarios. Lastly, the influence of the physical infrastructure quality, represented by the different IB typologies, on the overall system disruption, is presented.

6.1. Probability distributions of disruption to school system

The resulting probabilities of the states of disruption variable T_{SYS} , as a function of flood and seismic hazard intensities are presented in Fig. 15a, for the baseline scenario of building typology, characterised by the physical fragility functions presented in Section 4.4. A query into the probability distributions of its parent nodes T_{PF} and T_{OF} is helpful to gain insight into the variation in T_{SYS} states, shown in Fig. 15b and c, respectively. Disruption states from the physical functionality reduction (T_{PF}) varies predominantly with seismic hazard intensities, as the influence of flood hazard intensities on the structural damage is limited, (Fig. 12). The 100% probability of DD_s from structural causes, at nil seismic intensity, rapidly decreases with increase in PGA, and becomes insignificant beyond 0.52 g PGA, while a DD_m of up to 3 months becomes the most probable (95%) state for the system. The probability of DD_l up to 1 year increases gradually with PGA, with a maximum of 7.5% at the highest considered PGA, due to its low probability of occurrence, as per the hazard probability function used.

On the other hand, disruption from non-structural functionality loss T_{OF} , measuring the disruption from accessibility loss and change of function to shelter, is more dependent on the flood hazard level. Over the range of flood intensity considered, the probability of DD_s drops to a minimum of 48%. It can be noted that the probability of *short and long disruption* from non-structural causes show modest variation over the range of PGA, correctly capturing that the increased structural damage associated with PGA renders the schools unsuitable for shelter function. Therefore the probability of the 3 different states of overall disruption of the system, shown in Fig. 15a, combines the independent trends of T_{PF} and T_{OF} , delivering short, medium and long disruption probabilities of 0.01%, 85.34% and 14.66% respectively, for the coexisting maximum value of the two hazards.

Fig. 15d presents the modification in the distribution of system disruption, by considering the effect of social vulnerability ($T_{SYS,SV}$). Given the probability distributions assigned to the root variables IE , C_i and P_i the DD_s reduces to 70% in absence of hazardous events, with a corresponding rise of 30% in the DD_m , when compared to the T_{SYS} . This is due to considering the social vulnerability (SV) as a hazard independent component. The most relevant result is that DD_l probability for the maximum value of the two hazards is 2.5 times higher than the baseline case. This comparison of T_{SYS} and $T_{SYS,SV}$ illustrates the sensitivity of the system to social vulnerability and highlights its influence for successful education delivery.

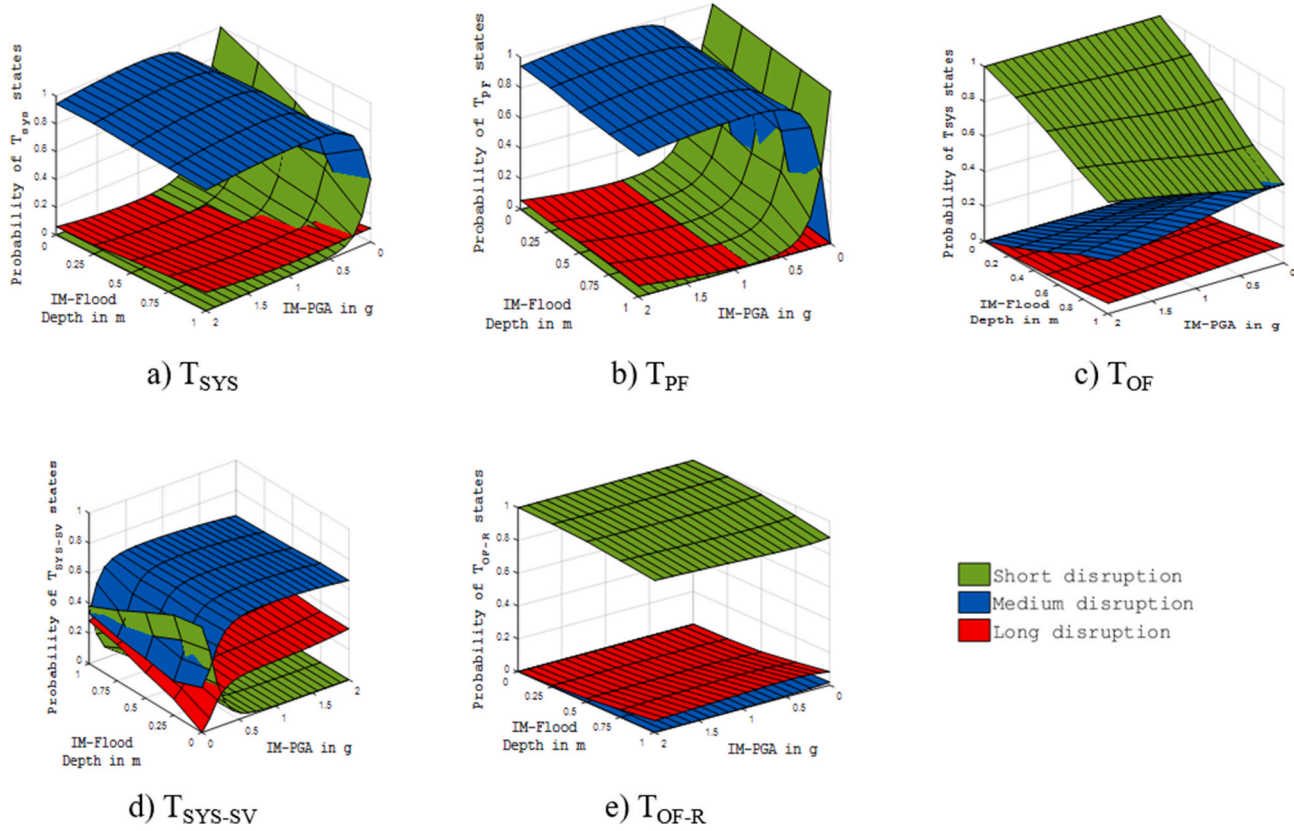


Fig. 15. Probability of T_{SYS} , T_{SYS-SV} and T_{OF-R} states for a base scenario.

The effectiveness of non-structural mitigation measures, such as the mobility of students between schools, can be assessed by comparing Fig. 15c and e, respectively depicting T_{OF} and the revised duration of disruption after considering mobility of students ($T_{OF,R}$). It can be seen that by allowing mobility between schools, the system can be maintained within the DD_s , i.e. 3 weeks, with at least 90% certainty. This is because the factors originally causing DD_m due to flood inundation can now be mitigated to DD_s , although the probability of DD_l is not reduced. Thus, mobility of students can have a substantial impact on education delivery in the event of floods. A reduction of the probability of DD_l (maximum 10%) requires structural interventions. A further estimation of revised system's disruption period T_{SYS-R} is performed assigning the same CPT definition of T_{SYS} , combining T_{PF} and $T_{OF,R}$ as shown in Fig. 16a. It can be seen that the combined system disruption is only modified along the flood hazard range at zero PGA when compared to Fig. 15a, as the non-structural mitigation is only effective for flood. The distribution along seismic hazard range is similar to that of the previous case, owing to the dependency of T_{SYS-R} on T_{PF} as per the CPT definition. A similar observation is made if the social vulnerability component is added to the T_{SYS-R} to obtain a revised $T_{SYS-SVR}$ as shown in Fig. 16b, and compared to T_{SYS-SV} in Fig. 15d, confirming the significant influence of SV. The BN thus allows to visualise and quantify the benefit of implementing simple mitigation strategies.

Table 15 summarise the probabilities of the states of the period of disruption variables, marginalised over the flood hazard range, concurrent to the maximum considered earthquake (MCE) PGA according to IS 1893, which is 0.36 g. Since the flood hazard characterization is based on a specific study of the region, and the whole range of intensity is relevant, the marginalisation is performed over the entire range. However, the range for seismic intensity is chosen sufficiently large to generate fragility curves for all the damage states, hence, the MCE level gives a more realistic notion of expected hazard intensities. The values give a direct quantification of system disruption for the given hazard characterization, building fragilities corresponding to the base case, and definitions of interconnections between hazards and exposures variables. The non-structural disruption has a 95% probability to be only up to 3 weeks, and non-structural mitigation further improves this chance. However, as the structural disruption is more likely to be up to 3 months, the overall disruption to the system also has a high probability to be medium duration. Inclusion of social vulnerability increases the chance of long disruption as mentioned previously, up to 25.8%. The marginal improvement in overall system disruption after non-structural mitigation at MCE level is also noted, although the effect was more significantly observed at zero PGA.

6.2. Sensitivity of system variables to contributing factors

The influence of the contributing parameters on system's disruption duration can be studied by setting the states of some parent nodes to a desired value and computing the updated probabilities of output variables. In order to illustrate the sensitivity of the system disruption variable T_{SYS} through Bayesian inference (see Appendix A), the estimated marginal probabilities of its three states are computed for three scenarios of practical significance:

1. One school's physical functionality after an event is (a) intact, possibly due to structural interventions prior to the event (i.e. PF_1 state = 1) and (b) shutdown, possibly due to structural damage during the event (i.e. PF_1 state = 3)
2. One school is (a) not used as a shelter (i.e. SH_1 state = 1) and (b) used as a shelter for over 3 months (i.e. SH_1 state = 4)
3. One school's inundation status is (a) not inundated, due to higher elevation (i.e. D_1 state = 1) and (b) inundated for more than a week (i.e. D_1 state = 4)

These evidence cases are provided to the BN to estimate the revised marginal probability over the flood hazard range at the PGA level of MCE, as shown in Fig. 17. The originally estimated marginal probabilities of T_{SYS} without evidence are included, showing that under the given hazard characteristics, T_{SYS} has about 15% and 85% probability of being in DD_s and DD_m , while a non-zero probability of DD_l exists. T_{SYS} shift for the 'case a' evidences for the three scenarios, i.e. state 1 for PF_1 , SH_1 and D_1 are indicated by green markers in Fig. 17, the red markers indicating the change caused by 'case b' evidence. For the first scenario (Fig. 17), $PF_1 = 1$ improves the probability of DD_s by 86%, while $PF_1 = 3$ leads to 99% probability of DD_m . Under scenario 2, $SH_1 = 1$ does not alter the original estimate significantly, but $SH_1 = 3$, produces a shift of T_{SYS} to DD_l , owing to the conditional probability definitions of OF_i . The duration

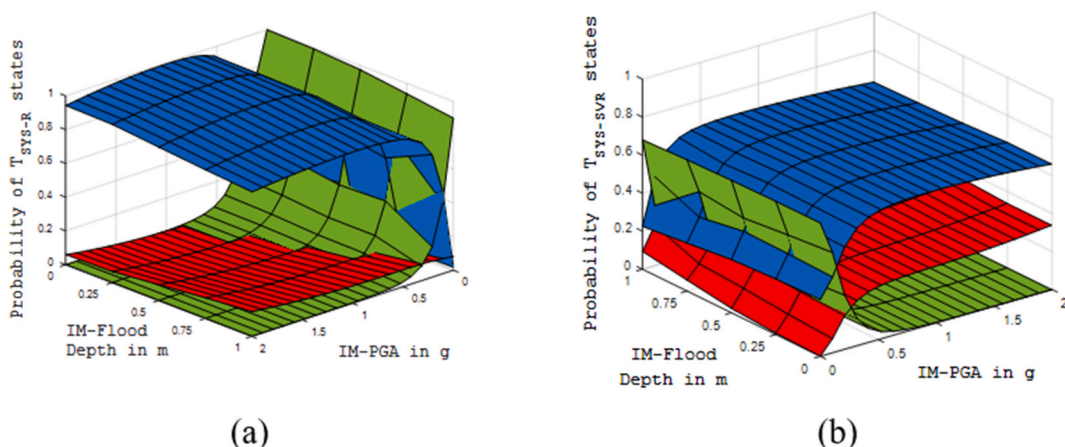
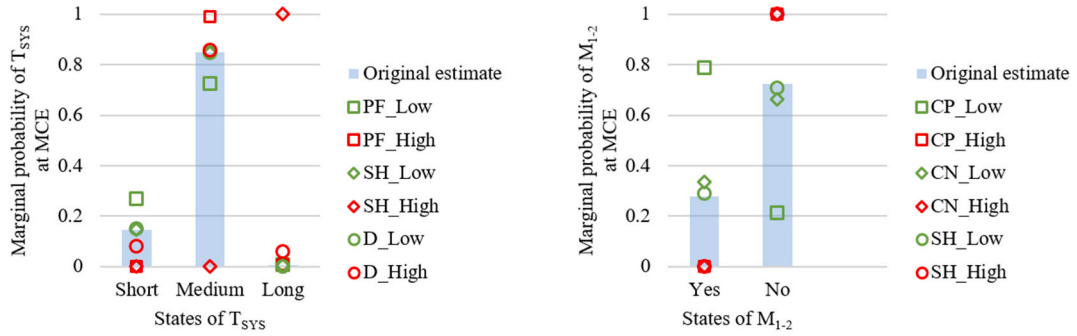


Fig. 16. a) Revised system disruption T_{SYS-R} with $T_{OF,R}$, b) $T_{SYS-SVR}$ while considering social vulnerability.

Table 15
Marginal probabilities of system outputs over the range of Flood hazard at MCE seismic hazard as per IS 1893.

States	T_{OF}	$T_{OF,R}$	T_{PF}	T_{SYS}	T_{SYS-SV}	$T_{SYS,R}$	$T_{SYS-SVR}$
1 Short (few weeks)	0.953	0.994	0.150	0.145	0.103	0.150	0.140
2 Medium (few months)	0.040	0.001	0.850	0.849	0.639	0.845	0.620
3 Long (1 year or more)	0.007	0.005	0.000	0.007	0.258	0.005	0.240



a) Effect of physical functionality, shelter function and duration of inundation at school site on system disruption (T_{SYS}) states

b) Effect of capacity, connectivity and shelter function on states of mobility between a pair of schools (M_{1-2})

Fig. 17. Influence of physical functionality, shelter function and inundation at site on duration of disruption of the school system.

Table 16
Assumed higher probability of flood hazard.

Flood depth (m)	0	0.25	0.50	0.75	1.0
Probability of exceedance	5%	35%	3%	2%	1%

of inundation at school site, D_1 has modest influence on the original estimate of T_{SYS} , compared to the other two factors, due to its limited control over OF_i states, and hence that of T_{SYS} states as defined by CPT of OF_i . It can be concluded that the SH_i state, which is also dependent on the PF_i state has a dominating influence on the states' probability of T_{SYS} .

A similar exercise is carried out to identify the most relevant parameter affecting the revised disruption period $T_{OF,R}$, determined by the mobility of students between schools. The extreme states (with same convention used in Fig. 17a) of the three root variable, school capacity (CP), connectivity (CN) and shelter function (SH) are considered and their relative influence on the two states of M_{1-2} is shown in Fig. 17b. Case b shows that the probability of M_{1-2} is solely dependent on the state of CN_{1-2} as shown in Table 13. The system also captures that high states of SH or CP will impede M_{1-2} . Conversely, 'Case a' comparison suggests that a state of $CP = 1$ improves the original M_{1-2} probability by more than 2.5 times, under the given hazard characterization and system properties. Since CP is dependent on school's physical functionality, this highlights the need for robust infrastructure, even when the mitigation measures are non-structural.

It can be observed from Table 15 that without specific inference the non-structural disruption (T_{OF}) in the present hazards conditions, has a 95% probability of DD_s , which is improved by 4.5% when considering the possibility of students' mobility. It can be expected that the effectiveness of non-structural mitigation would be more significant in a case of frequent flood hazards. Considering the anecdotal evidence reported in Section 3, the hazard characterization of the city is modified to reflect a higher probability of exceedance of flood depths as given in Table 16. The T_{OF} and $T_{OF,R}$ probability distributions assume the values shown in Fig. 18 to be compared with Fig. 15c and e. In this case, the marginal probabilities of T_{OF} and $T_{OF,R}$ over the range of flood depths at the MCE level of PGA, to be in the DD_s is 72.15% and 96.34% respectively, i.e. 33.5% improvement is achieved by the non-structural mitigation.

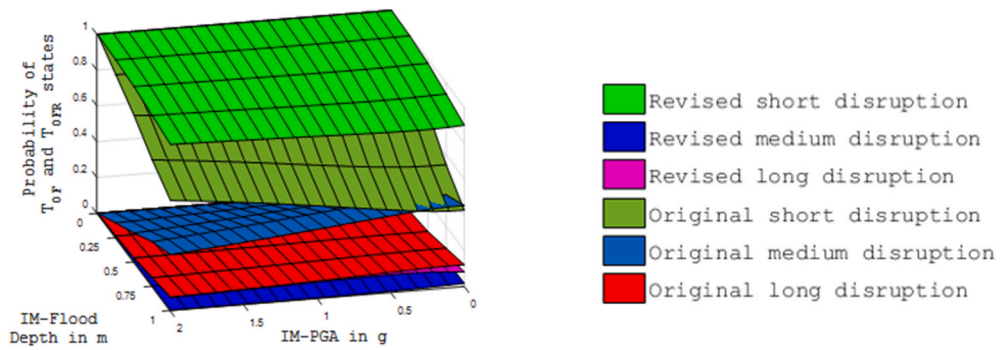


Fig. 18. Original and revised non-structural disruption at a fictitious high flood hazard case.

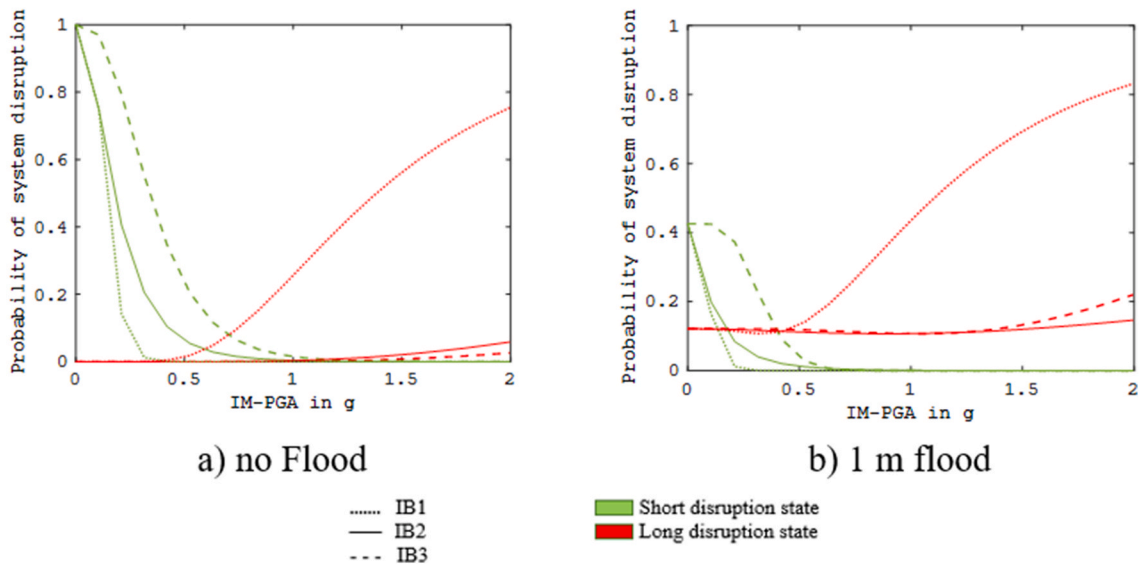


Fig. 19. Influence of building typology on system disruption.

6.3. Sensitivity to building typology

The analysis presented in the previous sections assumed a baseline scenario where buildings in all the schools were set as IB2 typology. The influence of building typology on system disruption (T_{SYS}) can be inferred from the BN analysis, by assigning the specific fragility functions summarised in Fig. 12 and Table 5, with IB1 being the most fragile and IB3 most robust typology. Results are

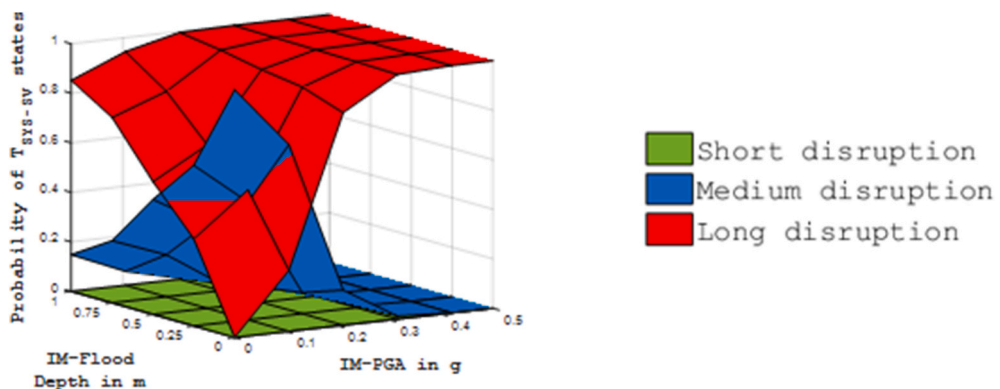


Fig. 20. System disruption for a scenario with high social vulnerability and poor typology of buildings.

presented as 2D plots in Fig. 19a and Fig. 19b, for DD_s and DD_l , assuming three cases, whereby all buildings belong to one of the three typologies.

The probability of DD_s falls from 45% to practically zero when considering IB3 and IB1, respectively, for PGA corresponding to MCE. Similarly, the probability of DD_l increases by 100%, although the values are insignificant at MCE level. At high PGA levels, the difference between IB1 and the other two typologies, which show comparable performance, increases. The 1 m flood depth results in an almost constant shift of the probability of DD_l by about 15%, due to flood related causes, irrespective of the typology. This also results in a reduction of up to 60% in the probability of DD_s , compared to the no-flood case. The likelihood of disruption is dominated by the seismic action rather than the flood depth at higher PGA ranges. However, at very high PGA level, the IB3 typology has a higher probability of DD_l than IB2, due to the former lower ductility for high flood depth, as noted in Section 4.4, under combined-hazard loading.

Communities of poor social and economic status may also be users of poorer building typology due to various reasons, such as lack of funds for maintenance and up keeping of schools. Assuming a scenario with high state of social vulnerability and all buildings of IB1 typology, the overall disruption could be further aggravated as measured through $T_{SYS,SV}$ shown in Fig. 20. There is no probability of the system being in DD_s under the given scenario. The system's probability of DD_m drops from 100% to 15% with the increasing flood hazard intensity alone. The probability of DD_l reaches 100% for a combination of 1 m flood and a PGA as low as 0.21 g. $T_{SYS,SV}$ has a 100% probability of DD_l for the MCE PGA value irrespective of the flood depth. Thus, combined effect of high social vulnerability and poor infrastructure results in a substantially more vulnerable scenario when compared with Fig. 15d.

7. Conclusion

School infrastructure plays a critical role in delivering education and supporting social cohesion in communities. In location of high natural hazards and social vulnerability, such role becomes indispensable as schools are also used as shelters in the emergency and recovery phase from a destructive event. Studies on the effects of concurrent natural hazards on the structural resilience of school infrastructure built with modest level of engineering are lacking. In response, the methodology developed in this study derives first, a set of robust fragility functions for confined masonry school buildings' physical vulnerability. Exploiting a novel modelling approach, it accounts for the recurring and sequential nature of demand arising from the geographic co-existence of flood and seismic hazard. A Bayesian network model underpins the second step of the methodology, by mapping the complex probabilistic resilience assessment of a system of several schools exposed to dual hazards scenarios, in terms of duration of disruption of system functionality due to physical vulnerability of the assets, accessibility of the compounds, changes in use to shelter, social vulnerability of the users' community and student population.

The analysis illustrates that BN is suitable to model the multi-hazard resilience assessment problem, containing qualitative and quantitative information, with discrete and continuous probability distributions. In particular, the inclusion of variables representing the social status of the users' community allows to quantify the relevance of social vulnerability, even though this is represented in a simple and qualitative way. The results are limited by the availability of specific elements of data, from the modest characterisation of the hazards, to the lack of resolution of the social variables. Nonetheless, the methodology is robust and allows to account for and propagate the uncertainties through the system (as can be quantified by methods such as proposed by Ref. [126]) enabling a probabilistic assessment of the disruption to the system. More nuanced results can be obtained with better data resolution, such as detailed flood basin characteristics, student demographics, distance between schools, seismicity at the sites, etc.

The BN modelling also allows to explore the effect of simple mitigation policies, such as mobility between schools [84] or selected use of schools as shelter. It is seen that the mobility has a beneficial effect on reducing the probability of *medium disruption*. This type of decision can be taken in the immediate aftermath of a disruptive flood event, once accessibility and shelter function of schools are agreed, within a district, to minimise loss of education days for students, and highlights the importance of considering schools as a system of connected infrastructure, to serve their communities. Similar mitigation measure could be extended for reducing disruption in the immediate aftermath of seismic events as well.

The analysis also illustrated the modelling of explicit relationships between variables and how their influence can be quantified in a probabilistic manner, over the entire hazard range. For instance, it was found that among the three contributing variables physical functionality, shelter function and inundation at school site, the shelter function has more influence on the overall disruption to the education system, providing evidence to current debate on the role of schools as shelters (e.g. Ref. [127]). Similarly, the building typology is also shown to considerably influence the probabilities of system disruption, and therefore the model is able to demonstrate the benefit of retrofit of existing school buildings to deliver more resilient infrastructure. The analysis is also able to quantify the level of risk associated to the two hazards and can therefore be helpful in decision making to prioritise action for structural or environmental interventions for different schools.

The study illustrated the analysis results of a system containing three schools or clusters, computationally very efficient. However, the challenge of extending the network for a large number of schools in a full regional network, while feasible, needs further exploration with respect to computational optimization.

Funding declaration

The study is made possible by financial support in the form of a Graduate-Overseas Research Scholarship awarded by University College London, supporting the PhD programme of the first author.

Declaration of competing interest

The authors declare that they have no known competing financial interests or personal relationships that could have appeared to influence the work reported in this paper.

Acknowledgement

Contribution and assistance from Dr Jayanta Pathak from Assam Engineering College and Assam State Disaster Management Authority, towards data collection of school buildings in Guwahati are gratefully acknowledged.

Appendix A. Bayesian inference

The process of Bayesian inference involves computing the complete probability distribution of a set of unobserved or hidden variables, given a set of observed variables in the Bayesian network. This can be achieved by updating the information of one or more observed nodes of the BN, i.e. by specifying the state or probability of certain nodes, to get the updated probability of other nodes in the network. For any general BN, with X representing the set of all n variables in the network, the inference of a set of variables X_i , given a set of variables X_j , can be expressed using conditional probability:

$$P(X_i|X_j) = \frac{P(X_i, X_j)}{P(X_j)} \tag{A.1}$$

where $P(X_i, X_j)$ is the joint probability of X_i and X_j and $P(X_j)$ is the probability of the observed variables. $P(X_i, X_j)$ can be estimated by summing all other variables in the network, X_k , from the joint probability of the whole network. Hence, Bayesian inference is to compute the following [128]:

$$P(X_i|X_j) = \alpha \cdot P(X_i, X_j) \propto \sum_{k \neq i, j} P(X_i, X_j, X_k) \tag{A.2}$$

This operation requires to formulate the joint probability $P(X) = P(X_i, X_j, X_k)$ in a computationally efficient manner. BN model facilitates this computation through factorization using the DAG structure and CPTs defined for each variable, as follows [129]:

$$P(X) = \prod_{i=1}^n P(X_i | Parents [X_i]) \tag{A.3}$$

For example, in a sample network of five nodes as shown in Figure A1, the joint probability is.

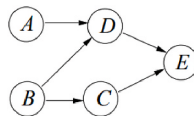


Fig. A.1. A sample Bayesian network (adapted from Ref. [89]).

$$P(A, B, C, D, E) = P(A)P(B)P(C|B)P(D|A, B)P(E|C, D) \tag{A.4}$$

For a BN with nodes representing variables with discrete states, as in this study, an exact inference is possible using a junction-tree algorithm, which works by finding ways to decompose the calculation of joint probability distribution into a linked set of local computations [130]. A junction-tree algorithm progresses through the following steps: 1) The DAG structure is first moralised by linking parents of all child nodes. 2) Variables are eliminated one at a time by an order obtained through partial optimization technique [89], until the whole graph is exhausted. When a node is eliminated, its adjacent nodes are connected through fill-in edges, if they are not previously connected and the eliminated node forms a ‘clique’ with its adjacent nodes (Figure A2) A junction tree is formed by the cliques and separators generated, following the junction-tree properties [130] to ensure global consistency of the network. Separators are sets of variables between two sets of nodes (or cliques), such that the two sets of nodes are conditionally independent, given the separator set. 4) Joint probabilities of each clique or ‘clique potential’ and separator sets are computed following the junction-tree.

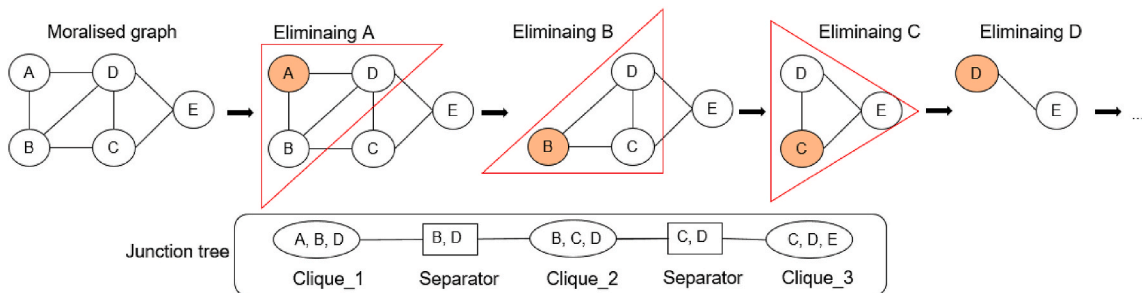
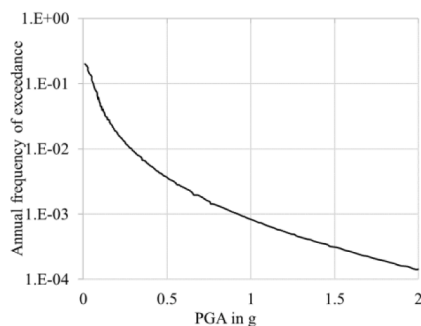


Fig. A.2. Steps 1–3 of Junction tree algorithm illustrated for a sample network (adapted from Ref. [89]).

Appendix B. Prior probabilities of seismic and flood hazards



a) Seismic hazard curve, in terms of annual exceedance frequency of PGA [109]

Flood depth (m)	Annual frequency of exceedance
0.25	8.6%
0.50	5.8%
0.75	2.9%
1.00	1.0%

b) Flood hazard data in terms of flood depth corresponding to 4 return periods [102]

References

- [1] M.C. de Ruiter, A. Couasnon, M.J.C. van den Homberg, J.E. Daniell, J.C. Gill, P.J. Ward, Why we can no longer ignore consecutive disasters, *Earth's Future* 8 (2020), <https://doi.org/10.1029/2019EF001425>.
- [2] UNISDR, Sendai Framework for Disaster Risk Reduction 2015 - 2030, [rr.org/uploads/Sendai_Framework_for_](http://www.wcdrr.org/uploads/Sendai_Framework_for_Disaster_Risk_Reduction_2015-2030.pdf), 2015, http://www.wcdrr.org/uploads/Sendai_Framework_for_Disaster_Risk_Reduction_2015-2030.pdf.
- [3] IS1893, Indian Standard: Criteria for Earthquake Resistant Design of Structures, Bureau of Indian Standards, no. June. Bureau of Indian Standards, 2002.
- [4] S.K. Jain, Indian earthquakes: an overview, *Indian Concr. J.* 72 (11) (1998) 555–562.
- [5] C. Murty, *Earthquake Tips*, Indian Institute of Technology Kanpur, 2005.
- [6] D.K. Bora, V. Sokolov, F. Wenzel, Validation of strong-motion stochastic model using observed ground motion records in north-east India, *Geomatics, Nat. Hazards Risk* (2014) 1–21, <https://doi.org/10.1080/19475705.2014.960011>, 0, no. 0.
- [7] J. Pathak, Status Survey of School & Hospital Buildings in Guwahati City Vol II-Restoration and Retrofitting Advisory," Assam State Disaster Management Authority, (ASDMA) Department of Civil Engineering, Assam Engineering College (AEC), 2014.
- [8] UN, Reducing Vulnerability of School Children to Earthquakes, United Nations Centre for Regional Development (UNCRD), 2009.
- [9] H.K. Miyamoto, A.S.J. Gilani, Damage Assessment and Seismic Retrofit of Heritage and Modern Buildings in the Aftermath of 2015 Nepal Earthquake, 2017.
- [10] K.S. Pribadi, et al., Learning from past earthquake disasters: the need for knowledge management system to enhance infrastructure resilience in Indonesia, *Int. J. Disaster Risk Reduc.* (2021).
- [11] J. Rodgers, *Why Schools Are Vulnerable to Earthquakes*, 2012.
- [12] S. Doocy, A. Daniels, S. Murray, T.D. Kirsch, The human impact of floods : a historical review of events 1980-2009 and systematic literature review, *PLOS Curr. Dis.* (2013) 1–30, <https://doi.org/10.1371/currents.dis.f4deb457904936b07c09daa98ee8171a> (Authors).
- [13] G. Forino, J. Von Meding, Child-Centred Risk Reduction Research-Into- Action Brief: Post-Disaster Educational Continuity in Urban Floods, *Global Alliance for Disaster Risk Reduction & Resilience in the Education Sector*, 2018.
- [14] S. Akello, Effects of Floods on Students Access to Secondary Education in Nyando District, Kisumu County, Kenya, University of Nairobi, 2014.
- [15] C. Mudavanhu, The impact of flood disasters on child education in Muzarabani district, Zimbabwe, *J. Dis. Risk Stud.* 6 (1) (2014) 1–8.
- [16] G.Y. Ardales, M.O. Victoria Espaldon, R.D. Lasco, M.T. Ana Quimbo, O.B. Zamora, Impacts of floods on public schools in the municipalities of Los Baños and bay, Laguna, Philippines, *J. Nat. Stud.* 15 (1) (2016) 19–40.
- [17] [savethechildren.org.uk](https://www.savethechildren.org.uk). <https://www.savethechildren.org.uk/news/media-centre/press-releases/children-out-of-school-as-south-asia-floods-put-education-at-risk>, 2017.
- [18] E. Munsaka, S. Mutasa, Flooding and its impact on education, in: *Natural Hazards-Impacts, Adjustments & Resilience-IntechOpen*, 2020.
- [19] Reliefweb, Hundreds of schools reopen after devastating floods in India. <https://reliefweb.int/report/india/hundreds-schools-reopen-after-devastating-floods-india>, 2018.
- [20] BBC, Chennai schools reopen after floods. <https://www.bbc.co.uk/news/world-asia-india-35090145>, 2015.
- [21] A. Bertho, D. Pande, P. Shrichand, S. Singh, Impact of Disasters on Children : A Case Study of Five Disaster-Prone Districts in Uttar Pradesh and Bihar , India, *Knowledge Community of Children in India*, 2012.
- [22] A. Anderson, K. McFarlane, M. Petal, S. Moli, Limiting and Planning for Schools as Temporary Evacuation Centres in Emergencies: Policy Brief and Practice Guidance for Pacific Nations in Support of the Worldwide Initiative for Safe Schools, *Asia Pacific Coalition for School Safety*, 2017.
- [23] Z. Wu, Y. Shen, H. Wang, M. Wu, Assessing urban flood disaster risk using Bayesian network model and GIS applications, *Geomatics, Nat. Hazards Risk* 10 (1) (2019) 2163–2184, <https://doi.org/10.1080/19475705.2019.1685010>.
- [24] R. Sinha, A. Goyal, A National Policy for Seismic Vulnerability Assessment of Buildings and Procedure for Rapid Visual Screening of Buildings for Potential Seismic Vulnerability, 2004.
- [25] World Bank, *Taxonomy Guide-GLOSI the, Global Library of School Infrastructure*, 2019.
- [26] F. Ceroni, N. Caterino, A. Vuoto, Simplified seismic vulnerability assessment methods : a comparative analysis with reference to regional school building stock in Italy, *Appl. Sci.* 10 (2020) 6771, <https://doi.org/10.3390/app10196771>.
- [27] S. Ruggieri, D. Perrone, M. Leone, G. Uva, M.A. Aiello, A prioritization RVS methodology for the seismic risk assessment of RC school buildings, *Int. J. Disaster Risk Reduc.* 51 (August) (2020) 101807, <https://doi.org/10.1016/j.ijdr.2020.101807>.
- [28] H. Azizi-Bondarabadi, N. Mendes, P.B. Lourenço, N.H. Sadeghi, Empirical seismic vulnerability analysis for masonry buildings based on school buildings survey in Iran, *Bull. Earthq. Eng.* 14 (11) (2016) 3195–3229, <https://doi.org/10.1007/s10518-016-9944-1>.
- [29] A.K. Sinha, A. Sinha, S. Singh, S. Kumar, Rapid seismic vulnerability assessment of school buildings, *Int. J. Civ. Eng. Technol.* 8 (2) (2017) 547–557.
- [30] UNCRD and SEEDS, Preliminary Survey and Assessment of Schools Buildings, UNCRD and Sustainable Environment and Ecological Development Society, 2008.
- [31] R. Dhungel, R. Guragain, N. Joshi, D. Pradhan, S.P. Acharya, Seismic Vulnerability Assessment of Public School Buildings in Nawalparasi and Lamjung District of Nepal, 2012.

- [32] A.M. Dixit, R. Yatabe, R.K. Dahal, N.P. Bhandary, Public school earthquake safety program in Nepal, *Geomatics, Nat. Hazards Risk* 5 (4) (2013) 293–319, <https://doi.org/10.1080/19475705.2013.806363>.
- [33] D. Gautam, R. Adhikari, R. Rupakhety, P. Koirala, An empirical method for seismic vulnerability assessment of Nepali school buildings, *Bull. Earthq. Eng.* 18 (13) (2020) 5965–5982, <https://doi.org/10.1007/s10518-020-00922-z>.
- [34] F. De Luca, N. Giordano, H. Gryc, L. Hulme, C. Mccarthy, *Nepalese School Building Stock and Implications on Seismic Vulnerability Assessment*, 2019.
- [35] N. Giordano, F. De Luca, A. Sextos, Analytical fragility curves for masonry school building portfolios in Nepal, *Bull. Earthq. Eng.* 19 (2) (2021) 1121–1150, <https://doi.org/10.1007/s10518-020-00989-8>.
- [36] R. Gentile, C. Galasso, Y. Idris, I. Rusydy, E. Meilianda, From rapid visual survey to multi-hazard risk prioritisation and numerical fragility of school buildings, *Nat. Hazards Earth Syst. Sci.* 19 (7) (2019) 1365–1386, <https://doi.org/10.5194/nhess-19-1365-2019>.
- [37] M. Zain, M. Usman, S.H. Farooq, T. Mehmood, Seismic vulnerability assessment of school buildings in seismic zone 4 of Pakistan, *Adv. Civ. Eng.* 2019 (2019), <https://doi.org/10.1155/2019/5808256>.
- [38] D. D' Ayala, et al., Resilient communities through safer schools, *Int. J. Disaster Risk Reduc.* (2020) 101446, <https://doi.org/10.1016/j.ijdrr.2019.101446>.
- [39] S. Ruggieri, F. Porco, G. Uva, D. Vamvatsikos, Two frugal options to assess class fragility and seismic safety for low-rise reinforced concrete school buildings in Southern Italy, *Bull. Earthq. Eng.* 19 (3) (2021) 1415–1439, <https://doi.org/10.1007/s10518-020-01033-5>.
- [40] G.J. O'Reilly, D. Perrone, M. Fox, R. Monteiro, A. Filiatrault, Seismic assessment and loss estimation of existing school buildings in Italy, *Eng. Struct.* 168 (April) (2018) 142–162, <https://doi.org/10.1016/j.engstruct.2018.04.056>.
- [41] NSET-Nepal and GHJ, *Seismic Vulnerability of the Public School Buildings of Kathmandu Valley and Methods for Reducing it*, National Society for Earthquake Technology, GeoHazards International (GHI), 2000.
- [42] OECD, "School Safety and Security, Keeping Schools Safe in Earthquakes, Proceedings of the Ad Hoc Experts' Group Meeting on Earthquake Safety in Schools, The OECD Programme on Educational Building, Paris, 2004.
- [43] T. Kabeyasawa, T. Kabeyasawa, K. Kusunoki, K. Li, An Outline of Damages to School Buildings in Dujiangyan by the Wenchuan Earthquake on May 12, 2008, 2008.
- [44] DRES, A Preliminary Report on School Buildings Performance during M 7.3 Ezgeleh, Iran Earthquake of November 12, 2017, Organization for Development, Renovation and Equipping Schools of I.R.Iran (DRES), 2017.
- [45] N. Giordano, F. De Luca, A. Sextos, F. Ramirez Cortes, C. Fonseca Ferreira, J. Wu, Empirical seismic fragility models for Nepalese school buildings, *Nat. Hazards* 105 (1) (2021) 339–362, <https://doi.org/10.1007/s11069-020-04312-1>.
- [46] C. Bhakuni, Seismic vulnerability assessment of school buildings, in: *SECED Young Engineers Conference 21-22 March 2005*, vol. 3, University of Bath, Bath, UK SEISMIC, 2005, pp. 553–557, 317.
- [47] C. Mudavanhu, The impact of flood disasters on child education in Muzarabani District, Zimbabwe, *Jamba J. Disaster Risk* 6 (1) (2014) 1–8, <https://doi.org/10.4102/jamba.v6i1.138>.
- [48] S.O. Ochola, B. Eitel, D.O. Olago, Vulnerability of schools to floods in Nyando River catchment, Kenya, *Disasters* 34 (3) (2010) 732–754, <https://doi.org/10.1111/j.1467-7717.2010.01167.x>.
- [49] A.A. Shah, et al., Reconnoitering school children vulnerability and its determinants: evidence from flood disaster-hit rural communities of Pakistan, *Int. J. Disaster Risk Reduc.* (2022) 102735, <https://doi.org/10.1016/j.ijdrr.2021.102735>.
- [50] M. Tomažević, I. Klemenc, Verification of seismic resistance of confined masonry buildings, *Earthq. Eng. Struct. Dynam.* 26 (10) (1997) 1073–1088, [https://doi.org/10.1002/\(SICI\)1096-9845\(199710\)26:10<1073::AID-EQE695>3.0.CO;2-Z](https://doi.org/10.1002/(SICI)1096-9845(199710)26:10<1073::AID-EQE695>3.0.CO;2-Z).
- [51] S. Brzev, *Earthquake-Resistant Confined Masonry Construction*, NICEE, National Information Center of Earthquake Engineering, 2007.
- [52] R. Meli, et al., *Seismic Design Guide for Low-Rise Confined Masonry Buildings*, Earthquake Engineering Research Institute, Oakland, California, 2011 no. August.
- [53] A. Chourasia, S.K. Bhattacharyya, P.K. Bhargava, N.M. Bhandari, Influential aspects on seismic performance of confined masonry construction, *Nat. Sci.* 5 (8) (2013) 56–62, <https://doi.org/10.4236/ns.2013.58a1007>.
- [54] A. Chourasia, S.K. Bhattacharyya, N.M. Bhandari, P. Bhargava, Seismic performance of different masonry buildings: full-scale experimental study, *J. Perform. Constr. Facil.* 26 (4) (2016) 371–376, [https://doi.org/10.1061/\(ASCE\)CF](https://doi.org/10.1061/(ASCE)CF).
- [55] S.M. Alcocer, J.C. Arce, D. Muria-Vila, L.R. Fernández-Sola, D.A. Guardia, Assessment of the seismic safety of school buildings in Mexico: a first look, 2, *suppl. Earthq. Spectra* 36 (2020) 130–153, <https://doi.org/10.1117/8755293020926184>.
- [56] A.P. Vatteri, D. D' Ayala, Classification and seismic fragility assessment of confined masonry school buildings, *Bull. Earthq. Eng.* (2021), 0123456789, <https://doi.org/10.1007/s10518-021-01061-9>.
- [57] I. Kelman, R. Spence, A limit analysis of unreinforced masonry failing under flood water pressure, *Masonry Int.* 16 (2) (2003) 51–61.
- [58] D.M. Herbert, An Investigation of the Strength of Brickwork Walls when Subject to Flood Loading (Thesis), Cardiff University, 2013.
- [59] D.M. Herbert, D.R. Gardner, M. Harbottle, T.G. Hughes, The Strength of Masonry Walls when Subject to Flood Loading, 2012.
- [60] R.B. Duarte, B.P. Sinha, Lateral strength of brickwork panels with openings, *Proc. Inst. Civ. Eng. Build.* 94 (4) (1992) 397–402.
- [61] R. Duarte, Design of unreinforced brickwork panels with openings under lateral pressure, *Mason. Int.* 11 (3) (1998) 97–101.
- [62] B. Haseltine, J. Tutt, Implications of research on design recommendations, *A. J. Inst. Struct. Eng.* 64 (1986) 341–350.
- [63] L. Milanese, M. Pilotti, A. Belleri, A. Marini, S. Fuchs, Vulnerability to Flash Floods: A Simplified Structural Model for Masonry Buildings, *Water Resour. Res.*, 2018, pp. 7177–7197, <https://doi.org/10.1029/2018WR022577>.
- [64] K. Meguro, H. Tagel-Din, Applied element method for structural analysis : theory and application for linear materials, *Struct. Eng. Eng. Jpn. Jpn. Soc. Civ. Eng.* 17 (1) (2000) 21–35.
- [65] S. Reese, D. Ramsay, *RiskScape : Flood Fragility Methodology*, New Zealand Climate Change Research Institute, 2010.
- [66] B. Merz, H. Kreibich, R. Schwarze, A. Thieken, Review article" Assessment of economic flood damage, *Nat. Hazards Earth Syst. Sci.* 10 (8) (2010) 1697–1724.
- [67] V. Stephenson, D. D' Ayala, A new approach to flood vulnerability assessment for historic buildings in England, *Nat. Hazards Earth Syst. Sci.* 14 (2014) 1035–1048, <https://doi.org/10.5194/nhess-14-1035-2014>.
- [68] D. D' Ayala, et al., Flood vulnerability assessment of urban traditional buildings in Kuala Lumpur, Malaysia, *Nat. Hazards Earth Syst. Sci.* (2020) 1–30, <https://doi.org/10.5194/nhess-2020-96>, no. April.
- [69] A. Mebarki, N. Valencia, J.L. Salagnac, B. Barroca, Flood hazards and masonry constructions : a probabilistic framework for damage , risk and resilience at urban scale, *Nat. Hazards Earth Syst. Sci.* 12 (2012) 1799–1809, <https://doi.org/10.5194/nhess-12-1799-2012>.
- [70] A. Blanco-Vogt, J. Schanze, Assessment of the Physical Flood Susceptibility of Buildings on a Large Scale – Conceptual and Methodological Frameworks, 2014, pp. 2105–2117, <https://doi.org/10.5194/nhess-14-2105-2014>.
- [71] D.F. D' Ayala, et al., Assessment of the multi-hazard vulnerability of priority cultural heritage structures in the Philippines (June, in: *ICONHIC*, 2016.
- [72] J. Dabbeek, V. Silva, C. Galasso, A. Smith, Probabilistic earthquake and flood loss assessment in the Middle East, *Int. J. Disaster Risk Reduc.* (2020), <https://doi.org/10.1016/j.ijdrr.2020.101662>.
- [73] M.C. de Ruyter, J.A. de Bruijn, J. Enghardt, J.E. Daniell, H. de Moel, P.J. Ward, The Asynergies of Structural Disaster Risk Reduction Measures: Comparing Floods and Earthquakes, *Earth's Futur.*, 2020, <https://doi.org/10.1029/2020EF001531>.
- [74] M.C. de Ruyter, P.J. Ward, J.E. Daniell, J.C.J.H. Aerts, Review article : a comparison of flood and earthquake vulnerability assessment indicators, *Nat. Hazards Earth Syst. Sci.* (2017) 1–34, <https://doi.org/10.5194/nhess-2017-45>.
- [75] B.E. Flanagan, E.W. Gregory, E.J. Hallisey, J.L. Heitgerd, B. Lewis, A social vulnerability index for disaster management, *J. Homel. Secur. Emerg. Manag.* 8 (1) (2011), <https://doi.org/10.2202/1547-7355.1792>.
- [76] M.K. Sen, S. Dutta, G. Kabir, Flood resilience of housing infrastructure modeling and quantification using a bayesian belief network, *Sustainability* 13 (3) (2021) 1–24, <https://doi.org/10.3390/su13031026>.

- [77] W. Utami, Study of social vulnerability as an effort on disaster risk reduction (study on suburban communities in Yogyakarta , Indonesia), IOP Conf. Ser. Earth Environ. Sci. 243 (2019), 012014, <https://doi.org/10.1088/1755-1315/243/1/012014>.
- [78] F. Fatemi, A. Ardalan, B. Aguirre, N. Mansouri, I. Mohammadfam, Social vulnerability indicators in disasters : findings from a systematic review, Int. J. Disaster Risk Reduc. 22 (2017) 219–227, <https://doi.org/10.1016/j.ijdrr.2016.09.006>.
- [79] I. Willis, J. Fitton, A review of multivariate social vulnerability methodologies: a case study of the River Parrett catchment, UK, Nat. Hazards Earth Syst. Sci. 16 (2016) 1387–1399.
- [80] L. Tascón-González, M. Ferrer-Julíà, M. Ruiz, E. García-Meléndez, Social vulnerability vssessment for flood risk analysis, Water 12 (2020) 558, <https://doi.org/10.3390/w12020558>.
- [81] I. Armaş, A. Gavriş, Social vulnerability assessment using spatial multi-criteria analysis (SEVI model) and the Social Vulnerability Index (SoVI model) – a case study for Bucharest, Romania, Nat. Hazards Earth Syst. Sci. 13 (2013) 1481–1499.
- [82] A. Fothergill, L.A. Peek, Poverty and disasters in the United States : a review of recent sociological findings, Nat. Hazards 32 (2004) 89–110.
- [83] B.S. Lai, A. La Greca, Understanding the Impacts of Natural Disasters on Children, 2020.
- [84] E. Chuang, J. Pinchoff, S. Psaki, How Natural Disasters Undermine Schooling, Brookings, 2018, pp. 9–12.
- [85] P. Weber, G. Medina-Oliva, C. Simon, B. Iung, Overview on Bayesian networks applications for dependability , risk analysis and maintenance areas, Eng. Appl. Artif. Intell. 25 (4) (2012) 671–682, <https://doi.org/10.1016/j.engappai.2010.06.002>.
- [86] Y.Y. Bayraktarli, J. Ulfkjaer, U. Yazgan, M.H. Faber, On the application of Bayesian probabilistic networks for earthquake risk management, in: 9th International Conference on Structural Safety and Reliability (ICOSSAR 05), 2005, pp. 20–23.
- [87] M.T. Bensi, A Bayesian Network Methodology for Infrastructure Seismic Risk Assessment and Decision Support (Thesis), University of California, Berkeley, 2010.
- [88] P. Franchin, A. Lupoi, F. Noto, S. Tesfamariam, Seismic Fragility of Reinforced Concrete Girder Bridges Using Bayesian Belief Network, August 2015, 2016, pp. 29–44, <https://doi.org/10.1002/eqe>.
- [89] P. Gehl, Bayesian Networks for the Multi-Risk Assessment of Road Infrastructure (Thesis), University College, London, UK, 2017.
- [90] M.K. Sen, S. Dutta, J.I. Laskar, A hierarchical bayesian network model for flood resilience quantification of housing infrastructure systems, 04020060, ASCE-ASME J. Risk Uncertain. Eng. Syst. Part A Civ. Eng. 7 (1) (2021), <https://doi.org/10.1061/ajrua6.0001108>.
- [91] S. Huang, H. Wang, Y. Xu, J. She, J. Huang, Key disaster-causing factors chains on urban flood risk, MDPI L 10 (2021) 210, <https://doi.org/10.3390/land10020210>.
- [92] H. Joo, C. Choi, J. Kim, D. Kim, S. Kim, H.S. Kim, A bayesian network-based integrated for flood risk assessment (InFRA), Sustainability 11 (2019), <https://doi.org/10.3390/su11133733>.
- [93] P. Gehl, D. D'Ayala, Development of Bayesian Networks for the multi-hazard fragility assessment of bridge systems, Struct. Saf. 60 (2016) 37–46, <https://doi.org/10.1016/j.strusafe.2016.01.006>.
- [94] O.M. Nofal, J.W. van de Lindt, Minimal building flood fragility and loss function portfolio for resilience analysis at the community level, 8, Water (Switzerland) 12 (2020), <https://doi.org/10.3390/w12082277>.
- [95] R. De Risi, et al., From flood risk mapping toward reducing vulnerability: the case of Addis Ababa, Nat. Hazards 100 (1) (2020) 387–415, <https://doi.org/10.1007/s11069-019-03817-8>.
- [96] F. Jalayer, G.T. Aronica, A. Recupero, S. Carozza, G. Manfredi, Debris flow damage incurred to buildings: an in situ back analysis, J. Flood Risk Manag. 11 (2018) S646–S662, <https://doi.org/10.1111/jfr3.12238>, 2013.
- [97] GOA, River systems of Assam, Jun. 12, 2021, <https://waterresources.assam.gov.in/portlets/river-system-of-assam>, 2021.
- [98] GMC, "GMC Wards and Area Sabhas, Guwahati Municipal Corporation, Guwahati Development Department, Government of Assam, 2021. <https://gmc.assam.gov.in/portlets/gmc-wards-area-sabhas>. Sep.08 2021.
- [99] Google Maps, Guwahati City, <https://www.google.co.uk/maps/place/Guwahati,+Assam,+India/@26.1606966,91.7003114,12.5z/data=!4m5!3m4!1s0x375a5a287f9133ff:0x2bbd1332436bde32!8m2!3d26.1445169!4d91.7362365?hl=en>, Google Maps (online), 2021. Sep. 08, 2021.
- [100] NRSC, ISRO, and ASDMA, Flood Hazard Atlas for Assam State, 1998-2015, National Remote Sensing Centre, Indian Space Research Organisation, Dept. of Space, Govt. of India, 2016.
- [101] P. Barman, C. Goswami, Flood Zone Mapping of Guwahati Municipal Corporation Area Using GIS Technology, 2009.
- [102] S.N. Sahoo, P. Sreeja, Development of Flood Inundation Maps and Quantification of Flood Risk in an Urban Catchment of Brahmaputra River, ASCE-ASME J. Risk Uncertain. Eng. Syst., Part A: Civ. Eng. 3 (1) (2017) 1–11, <https://doi.org/10.1061/AJRU6.0000822>.
- [103] D. Chakraborty, M. Singh, Development and urban flooding, case-Guwahati, J. Basic Appl. Eng. Res. 3 (12) (2016) 1081–1086.
- [104] ASDMA, Review of Studies on Urban Floods in Guwahati from Flood Knowledge to Urban Action, All India Disaster Mitigation Institute (AiDMI), 2014.
- [105] T. Sarmah, S. Das, Urban flood disaster assessment for Guwahati city, in: International Symposium on Water Urbanism and Infrastructure, 2017 (no. January).
- [106] GMC, Flood-free Guwahati. <https://gmc.assam.gov.in/frontimpotentdata/flood-free-guwahati>, 2021. (Accessed 25 May 2021).
- [107] P. Barman, B. Sarma, A. Sarma, A Study on Flood Hazard Mitigation of Guwahati City, Asian Rev. Civ. Eng., 2012.
- [108] A. Menon, T. Ornthamarath, M. Corigliano, C.G. Lai, Probabilistic seismic hazard macrozonation of Tamil Nadu in southern India, Bull. Seismol. Soc. Am. 100 (3) (2010) 1320–1341, <https://doi.org/10.1785/0120090071>.
- [109] S.K. Nath, K. Thingbaijam, Probabilistic seismic hazard assessment of India, Seismol Res. Lett. 83 (1) (2012) 135–149, <https://doi.org/10.1785/gssrl.83.1.135>.
- [110] M. Sharma, S. Malik, Probabilistic Seismic Hazard Analysis and Estimation of Spectral Strong Ground Motion on Bed Rock in Northeast India, 2006.
- [111] A.K. Mahajan, V.C. Thakur, M.L. Sharma, M. Chauhan, Probabilistic seismic hazard map of NW Himalaya and its adjoining area , India, Nat. Hazards 53 (2010) 443–457, <https://doi.org/10.1007/s11069-009-9439-3>.
- [112] ELS, Extreme Loading ® for Structures Theoretical Manual, Applied Science International, LLC, 2004.
- [113] H.B. Kaushik, D.C. Rai, S.K. Jain, Stress-strain characteristics of clay brick masonry under uniaxial compression, J. Mater. Civ. Eng. 19 (9) (2007) 728–739, [https://doi.org/10.1061/\(ASCE\)0899-1561\(2007\)19:9\(728\)](https://doi.org/10.1061/(ASCE)0899-1561(2007)19:9(728)).
- [114] C.P. Choudhury, J. Pathak, Analytical Study of Seismic Response of Traditional Assam-type Housing in North-East India, 2014.
- [115] V. Stephenson, D. D'Ayala, Structural response of masonry infilled timber frames to flood and wind driven rain exposure, J. Perform. Constr. Facil. 33 (3) (2019), [https://doi.org/10.1061/\(ASCE\)CF.1943-5509.0001281](https://doi.org/10.1061/(ASCE)CF.1943-5509.0001281).
- [116] IS456, Indian Standard: Plain and Reinforced Concrete- Code of Practice, Bureau of Indian Standards." Bureau of Indian Standards, India, 2000.
- [117] P. Fajfar, A non-linear analysis method for performance-based seismic design, Earthq. Spectra 16 (3) (2000) 573–592.
- [118] FEMA_P695, Quantification of Building Seismic Performance Factors. Federal Emergency Management Agency (FEMA), American Society of Civil Engineers, 2009.
- [119] S.P. Simonovic, Civil Engineering Systems- Course Notes, the University of Western Ontario, The University of Western Ontario, London, 2003.
- [120] J. Kinghorn, How long does it take to recover from an earthquake? AIR Worldwide (2017). <https://www.air-worldwide.com/blog/posts/2017/4/how-long-does-it-take-to-recover-from-an-earthquake/>. (Accessed 23 September 2021).
- [121] A. Tsioulou, J. Faure Walker, D.S. Lo, R. Yore, A method for determining the suitability of schools as evacuation shelters and aid distribution hubs following disasters: case study from Cagayan de Oro, Philippines, Nat. Hazards 105 (2) (2021) 1835–1859, <https://doi.org/10.1007/s11069-020-04380-3>.
- [122] J. Pathak, Status Survey of School and Hospital Buildings in Guwahati City Vol - I, Assam State Disaster Management Authority, ASDMA) Department of Civil Engineering, Assam Engineering College (AEC), 2014.
- [123] DES, Economic Survey Assam 2017-18, Government of Assam, 2018.
- [124] MMA, District Report Kamrup, Ministry of Minority Affairs Government of India, 2001.
- [125] DES, Economic Survey Assam 2011-12," Directorate of Economics and Statistics, Government of Assam, 2012.
- [126] B. Das, Representing Uncertainties Using Bayesian Networks, DSTO Electronics and Surveillance Research Laboratory PO, 1999.

- [127] J.J. Wang, Study on the context of school-based disaster management, *Int. J. Disaster Risk Reduc.* 19 (2016) 224–234, <https://doi.org/10.1016/j.ijdr.2016.08.005>.
- [128] K.P. Murphy, The Bayes Net toolbox for matlab, *Comput. Sci. Stat.* 33 (2) (2001) 1024–1034.
- [129] J. Xue, Applied Bayesian Methods, Taught Course in the Department of Statistical Science, UCL, London, 2018.
- [130] M.I. Jordan, The Junction Tree Algorithm, "UC Berkeley Electrical Engineering and Computer Science, *Statistical Learning Theory Course*, 2004, pp. 1–5.